Photocatalytic CO_2 Reduction Using Manganese and Rhenium Catalysts Containing Bidentate Phosphinoaminopyridine Ligands

Sarah Osterholm

Thesis submitted to the University of Ottawa
in partial fulfillment of the requirements
For the degree of
Master of Science in Chemistry

Department of Chemistry and Biomolecular Science

Faculty of Science

University of Ottawa

Abstract

CO_2 is generally regarded as a waste product. However, the efficient catalytic reduction of CO_2 means that this concept can change to viewing this molecule as a feedstock to produce chemically valuable products. The catalytic reduction of CO_2 is a challenge because of its stability, and its reduction into chemically valuable products requires an appropriate catalyst and accessible energy source. While second and third row transition metals have shown considerable promise as photocatalysts for the reduction of CO_2 to CO, one of our goals is to elaborate on the metal centers and the ligand environments in order to discover new catalysts and processes. These efforts have revealed new photocatalysts based on manganese and rhenium supported by κ^2-PN phosphinoaminopyridine ligands. This thesis will describe the synthesis and characterization of these catalysts and their CO_2 reduction parameters. The selectivity of these catalysts for either CO or HCOOH will be explored. Furthermore, ligand modifications and their effects on the catalyst behaviour will also be presented.

Acknowledgements

Firstly, I would like to thank my supervisor, Dr. Darrin Richeson, for accepting me into the Richeson group. I have had an amazing 3 and a half years with this group during both undergraduate and graduate research and I have learned so much from everyone. I would also like to thank all the members of the Richeson group, past and present, who I have worked with over the years. Special thanks go to Somayeh Norouziyan, Josh Brown, Patrick Berro, and Sara Ahmadi who have all helped me and supported me throughout my years in the Richeson lab. A shout out also goes to the Bryce Lab for their continued support and lending of equipment throughout the years, and especially to Vince Morin who has not only lent equipment but also advice and guidance on all things NMR and crystals. I will miss the Bricheson Lab (Bryce-Richeson) joint social gatherings and involvement in every chemistry department activity like BBQs, scavenger hunts, and mixers as the Bricheson team.

I would also like to acknowledge other members of the department who have helped with my research. Both Dr. Bulat Gabidullin and Dr. Jeffrey Ovens have provided single crystal X-ray analysis, Dr. Sharon Curtis has provided mass spectrometry analysis for several complexes throughout this thesis, and Dr. Wendy Pell has allowed us to use the GC and has always been helpful and supportive in answering any questions regarding chemistry.

I also want to thank my amazing family, my parents and my sister, for their emotional support over the years even if they never understood what I was talking about when I try to explain my research to them! To be able to pursue my passion of chemistry with the total and unwavering support of my family is the greatest dream come true. And of course, my partner John, who has supported me in my academic career since I began my journey into grad school and who has always encouraged me when I feel disheartened or overwhelmed.

Without the support of everyone here I would have never been able to complete my journey and finish my master's degree. I have thoroughly enjoyed my years as a member of the department of chemistry at the University of Ottawa and as a member of the Richeson Lab. After 8 years in the department of chemistry and 3.5 years in the Richeson Lab it will be hard to say goodbye to this chapter of my life and move on to the next stage, which is hopefully employment!

Table of Contents

Chapter 1: Introduction

List of Tables

List of Figures

List of Schemes

List of Abbreviations

ACN	Acetonitrile
bpy	2,2’-bipyridine
Cat	Catalyst
CS	Catalytic Selectivity
DCM	Dichloromethane
DMA	Dimethylacetamide
DMF	N,N-dimethyl formamide
ED	Electron Donor
PN	Phosphinoaminopyridine
PS	Photosensitizer
S	Solvent
TM	Transition Metal
TON	Turn Over Number
TOF	Turn Over Frequency
TEA	Triethylamine
TEOA	Triethanolamine
THF	Tetrahydrofuran

Chapter 1: Introduction

In this thesis, the photochemical reduction of CO_2 using transition metal catalysts bearing bidentate phosphinoaminopyridine ligands will be explored. The PN ligands will be modified, as well as the metal centers, in order to investigate different catalysts. The selectivity of these selected catalysts will be explored and compared to previously reported CO_2 reduction catalysts. Chapter 1 will detail all relevant background information in order for the reader to understand the work presented in this thesis. Chapter 2 will focus on the synthesis and characterization of all ligands and complexes used in this thesis. The third chapter will focus on the photochemical reactions and the results obtained.

1.1 General Introduction

A critical challenge that faces the world today is environmental pollution. Currently, one of the most used energy sources is fossil fuels, which are rapidly consumed because of increasing energy demands. The combustion of fossil fuels results in the generation of carbon dioxide (CO_2), which is a major greenhouse gas. Fossil fuel combustion is a central contributor to the high levels of atmospheric carbon dioxide.[1, 2] An important area of research in recent decades has been the reduction of the atmospheric CO_2 levels to produce more valuable products. A photochemical approach to reduction of carbon dioxide is desirable because the required energy input can be supplied from renewable sources such as solar energy. However, there is a critical challenge in the area of CO_2 reduction, which is that in order to convert CO_2 to other valuable products, a large energy input is needed, which can lead to high production costs. To address this, research into new catalytic systems that are able to increase the efficiency of CO_2 transformation are very important.[2]

1.2 Thermodynamics of Carbon Dioxide Reduction

The reduction of carbon dioxide is a very challenging reaction, as CO_2 possesses strong C=O double bonds, with a bonding energy of 750 kJ/mol. This bonding energy is much larger compared to a C-C bond (336 kJ/mol) or a C-O bond (327 kJ/mol), making CO_2 a very stable molecule. The photocatalytic or electrocatalytic reduction of CO_2 requires significant energy to break the C=O bond. There are several different pathways through which CO_2 reduction may proceed, giving an array of reduction products including carbon monoxide (CO), formic acid (HCOOH), methane (CH_4), ethylene (C_2H_4), and others.[2] The reduction of CO_2 to $CO_2^{\cdot -}$ via direct one electron reduction is an unfavourable process, as shown by the large reduction potential of -2.14V vs SCE, as CO_2 is the most oxidized state of carbon.[3] There are other more favourable pathways which employ proton assisted multiple electron transfer, shown in Table 1.2. These proton coupled electron transfer reactions are more favourable than the one electron reduction reaction, shown by the smaller negative values.[4] The reduction potential values are related to Gibb's free energy by the equation: $\Delta G = -nFE°$, where n is the moles of electrons, F is the Faraday constant, and E° is the reduction potential. In order for a reaction to be spontaneous, ΔG should be negative, and so a positive E° value is desired.

Table 1.2. The CO_2 reduction potentials for various CO_2 reduction reactions.[4]

Reaction	E°(V) vs SCE*
$CO_2 + 2H^+ + 2e^- \rightarrow HCO_2H$	-0.85
$CO_2 + 2H^+ + 2e^- \rightarrow CO + H_2O$	-0.77
$CO_2 + 4H^+ + 4e^- \rightarrow C + 2H_2O$	-0.44
$CO_2 + 4H^+ + 4e^- \rightarrow HCHO + H_2O$	-0.72
$CO_2 + 6H^+ + 6e^- \rightarrow CH_3OH + H_2O$	-0.62
$CO_2 + 8H^+ + 8e^- \rightarrow CH_4 + 2H_2O$	-0.48

*E° potential reported at pH 7.

Proton coupled electron transfer reduction is more thermodynamically favourable, but it requires a catalyst. Transition metal compounds are widely used as catalysts for these reactions, as these catalysts can have multiple redox states which can help to promote multiple electron transfer. Transition metal compounds can be used as homogeneous catalysts in order to overcome the kinetic limitations of the proton coupled electron transfer reduction by promoting the multiple electron transfer reactivity of the reduction reaction. As well, the formal reduction potentials can be tuned in order to match the potential required for CO_2 reduction by modifying the ligand. Many different catalysts using transition metals have been employed to reduce CO_2, consisting of the central metal and organic based ligands.[4]

1.3 Photochemical Carbon Dioxide Reduction

In the 1970's and 1980s studies on photocatalytic CO_2 reduction started. Halmannn, in 1978, observed that under light illumination, CO_2 was reduced to CH_3OH and CO on a p-type GaP electrode. The next year, Inoue *et al* observed that formic acid, formaldehyde, and methyl alcohol were produced from the photocatalytic reduction of CO_2 in aqueous suspensions of semiconductors such as TiO_2 and ZnO. In the decades since these pioneering experiments, scientists have increasingly studied the photocatalytic reduction of CO_2 using different catalysts. Photocatalytic reduction of carbon dioxide by using the energy of sunlight combined with homogeneous transition metal catalysts is an attractive process to address the energy and environmental issues of carbon dioxide emissions. A photochemical approach to reduction of carbon dioxide is desirable because the required energy input can be supplied from renewable sources such as solar energy. Transforming carbon dioxide to more valuable products such as CO, HCOOH, CH_4, alcohols, and aldehydes is a challenge because of the need to control the CO_2 reduction pathways for the products.[2,5]

1.3.1 Components for a Photocatalytic Reduction System and Performance Parameters

In order for a photocatalytic system to work, there are several components that are needed, including the catalyst (Cat), the photosensitizer (PS), the electron donor (ED), and the solvent (S). When looking at the productivity or efficiency of a photocatalytic system, parameters such as catalytic selectivity, quantum yield (φ), turn over number (TON) and turn over frequency (TOF) are examined. These components and parameters will be explained below.

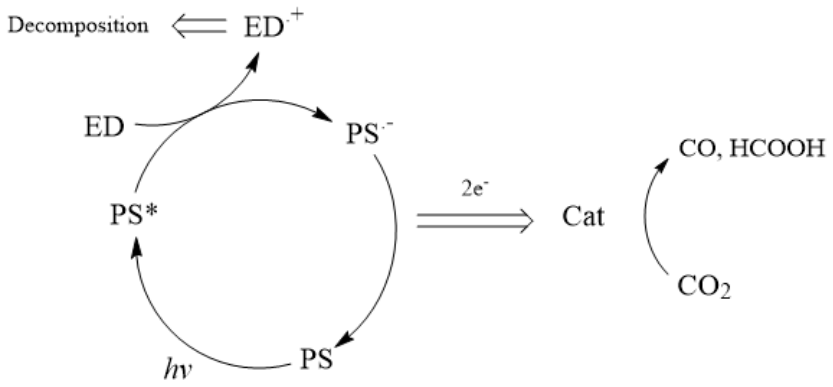

Scheme 1.3.1. Schematic reaction pathway for the photocatalytic multi-electron CO_2 reduction, where PS is the photosensitizer, ED is the electron donor, and Cat is the catalyst. [3]

1.3.2 Catalyst (Cat)

The core reaction site of a photocatalytic system is the catalyst.

Some of the important features a catalyst should possess are:

1. Redox activity (meaning the ability to transfer between different oxidation states)
2. Ability to quench the excited state of the PS (for oxidative quenching)
3. High solubility in various solvents
4. Stable
5. Inexpensive

6. Abundant materials
7. Low toxicity

As previously mentioned, transition metal compounds are widely used as homogeneous catalysts in the proton coupled electron transfer reduction of carbon dioxide. These catalysts can have multiple redox states, which can help to promote multiple electron transfer. Modifying the ligand can also help to tune the formal reduction potential in order to match the potential required for CO_2 reduction. Many different transition metal catalysts have been used to reduce CO_2, consisting of the central metal and organic based ligands. [3,4] Figure 1.3.2 represents some examples of transition metal catalysts that have been documented to reduce carbon dioxide.[3]

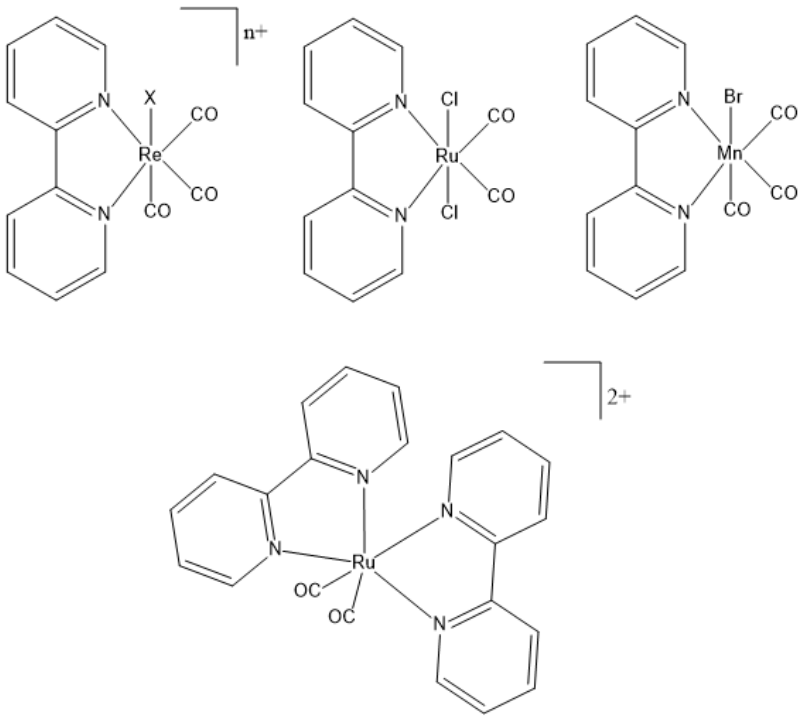

Figure 1.3.2. The structures of selected complexes that have been reported as catalysts for photocatalytic CO_2 reduction.[3]

1.3.2.1. Types of Catalysts for Photocatalytic Reduction of CO_2 (Type I vs Type II)

A homogeneous photocatalytic system consists of both a photosensitizer and catalyst. The relationship between these two components can be categorized into either Type I or Type II systems. Type I systems consist of two separate components, the photosensitizer and the catalyst, which are separate compounds that are mixed in the solution. Type II systems have the two components in a single molecular unit that functions as both the photosensitizer and catalyst.[4] These two types are explained in this section.

1.3.2.2 Type I Photocatalyst System

Type I catalysis is considered a photosensitized CO_2 reduction process. Type I catalysis consists of two separate components with one acting as the photosensitizer (PS), and one acting as the catalyst (Cat). During irradiation, the photosensitizer (PS) absorbs the light and is promoted to an excited electronic state. The excited state of the photosensitizer is quenched by the electron donor (ED) to form the reduced photosensitizer (PS^{-}) and the oxidized electron donor ($ED^{\cdot+}$). This reduced photosensitizer will transfer the electron to the catalyst (Cat) to produce the reduced catalyst (Cat^{-}) that will react with CO_2 to reduce it and produce the desired products.[4]

In the 1980s Tinnemans *et al* were the first to study $Ru(bpy)_3^{2+}$ sensitized CO_2 reduction by transition metal tetraaza-macro-cyclic compounds, $[M^{II}L]$. Carbon monoxide was identified as the CO_2 reduction product, however the main product was H_2, resulting in low selectivity.[6,7] Since Tinneman's primary research, other photosensitizers such as phenazine and p-terphenyl have also been studied with transition metal tetraaza-macro-cyclic compounds.[4,6] Another example of a Type I catalysis system uses transition metal complexes such as $[Mn^{I}(bpy)(CO)_3Br]$[7,8] (Figure 1.3.4), along with a photosensitizer such as tris(2,2'-bipyridine) ruthenium (II) and an electron donor such as TEOA, BNAH, or TEA.

1.3.2.3. Type II Photocatalyst System

Type II catalysis consists of a single compound that acts as both the catalyst and photosensitizer. After the photocatalyst (PScat) absorbs the light to be excited, the excited state of the photocatalyst will undergo reductive quenching with the electron donor (ED) to form the active state of the catalyst that is able to react directly with CO_2 and reduce it to more valuable products.[4,9] Type II catalysis systems have been reported for metalloporphyrins or the related metallo-macrocycles (Figure 1.3.2.3.1), and the rhenium complexes $Re^{I}(bpy)(CO)_3X$ (where X= Cl or Br). In addition, all of these Type II complexes can be used as catalysts for Type I with an appropriate photosensitizer.[4,9,10] Metalloporphyrins and related metallo-macrocycle catalysts that have been used to reduce CO_2 often use nickel, cobalt, and iron as the transition metal center.[6,11,12,13] Some examples of these metalloporphyrins are shown in figure 1.3.2.3.1.[4]

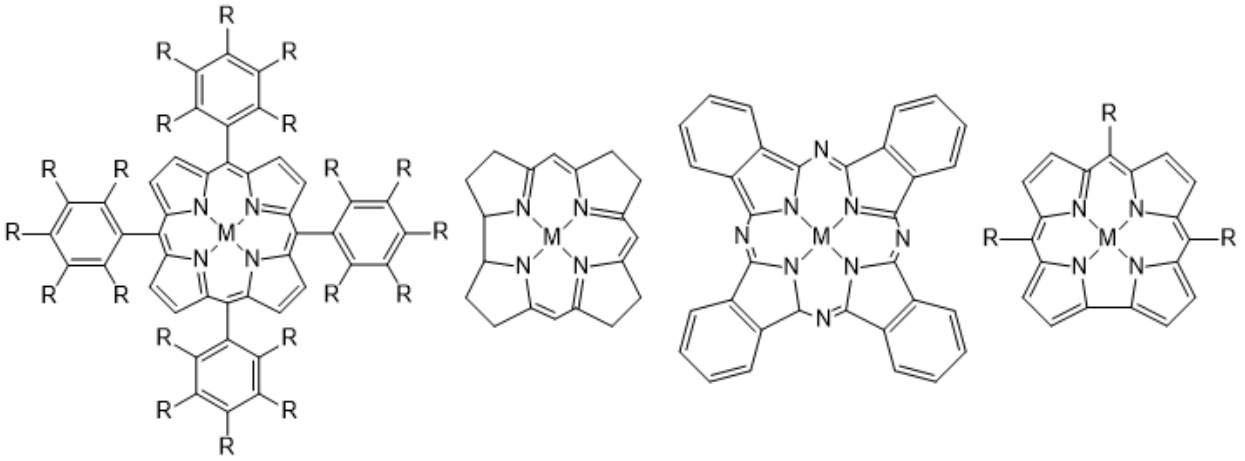

Figure 1.3.2.3.1. The structure of metal porphyrin derivatives and related metallo-macrocycles.[4]

In the early 1980's, it was discovered that *fac*-$[Re^{I}(bpy)(CO)_3Cl]$ was an effective Type II photocatalyst for CO_2 reduction, and this initiated investigations into the bpy framework in this field. These $Re^{I}(bpy)(CO)_3X$ complexes show high quantum efficiencies for their ability to reduce CO_2 selectively to CO.[4,9,10]

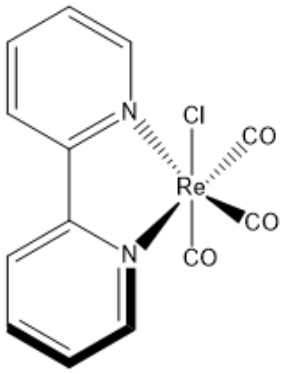

Figure 1.3.2.3.2 The structure of [Re^{I}(bpy)$(CO)_3$Cl] complex.

The Re(I) complexes [Re^{I}(bpy)$(CO)_3$(X)] (X= Cl or Br) reported by Hawecker, Lehn and coworkers were the first photocatalysts able to reduce CO_2 to CO.[4,9,10]

In 2011, the Mn(I) analogues were investigated. The reason for this is to shift to more abundant metals to replace the rare metals. The Mn(I) analogues were discovered to be good electrocatalysts in 2011, and good catalysts for photochemical CO_2 reduction in 2014. In photocatalytic CO_2 reductions, *fac*-[Mn^{I}(bpy)$(CO)_3$Br] (Figure 1.3.2.3.3) was reported as an efficient type I catalyst for CO_2 reduction, using $[Ru(dmb)_3]^{2+}$ (Figure 1.3.2.3.4) as a photosensitizer. It has shown both a good activity towards CO_2 reduction, and a good selectivity to produce formate.[3,8,14]

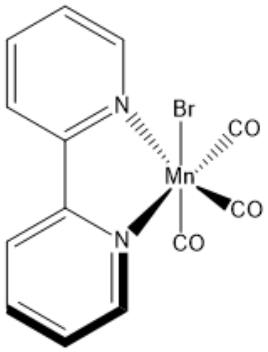

Figure 1.3.2.3.3. The structure of [Mn^{I}(bpy)$(CO)_3$Br] complex.

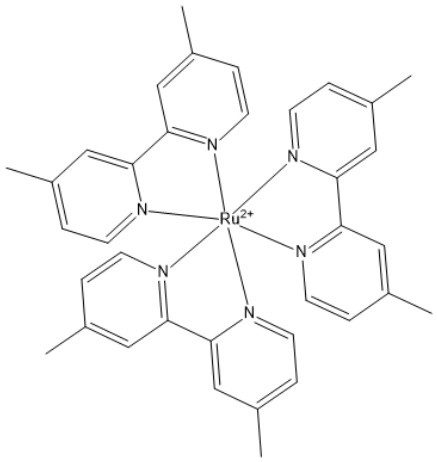

Figure 1.3.2.3.4. The structure of $[Ru(dmb)_3]^{2+}$ photosensitizer.

1.3.3 Electron Donor (ED)

The electron donor provides the electrons needed for the reduction reaction. The electrons are generally transferred to the catalyst using the photosensitizer as an intermediary. In the description of the photosensitizer (PS), the details of this process will be explained. When choosing an electron donor, there are several important factors that must be considered. The stability of the oxidized electron donor ($ED^{\bullet+}$) is important because it can affect the overall efficiency of the system. The efficiency can be reduced by back-electron transfer from the reduced excited state of the photosensitizer ($PS^{\bullet-}$) to the oxidized electron donor ($ED^{\bullet+}$). Another factor to consider is the reactivity of the oxidized electron donor and by-products. These species present in the system can interact with reaction intermediates and therefore decrease the efficiency of the intended reaction. Some commonly used electron donors for CO_2 reduction include triethanolamine (TEOA) and triethylamine (TEA), and their structures are presented in Figure 1.3.3. Both of these compounds have very low ionization energies, which is defined as the minimum amount of energy required to remove an electron, and so act well as electron donors. Also shown is a scheme for the possible mechanism of how TEOA works during the photocatalytic cycle.

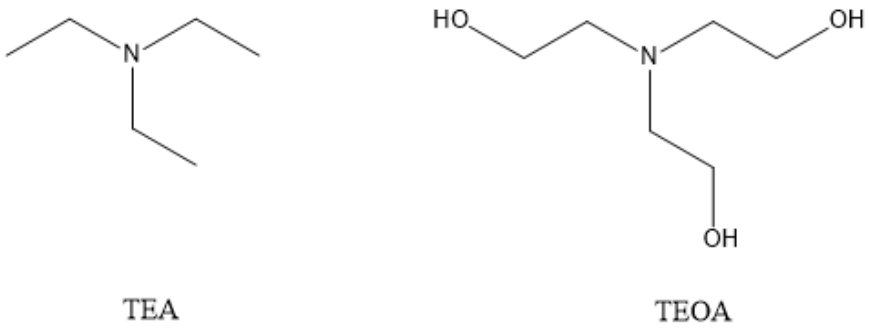

Figure 1.3.3. Structures of TEA and TEOA, common electron donors for photochemical reactions.

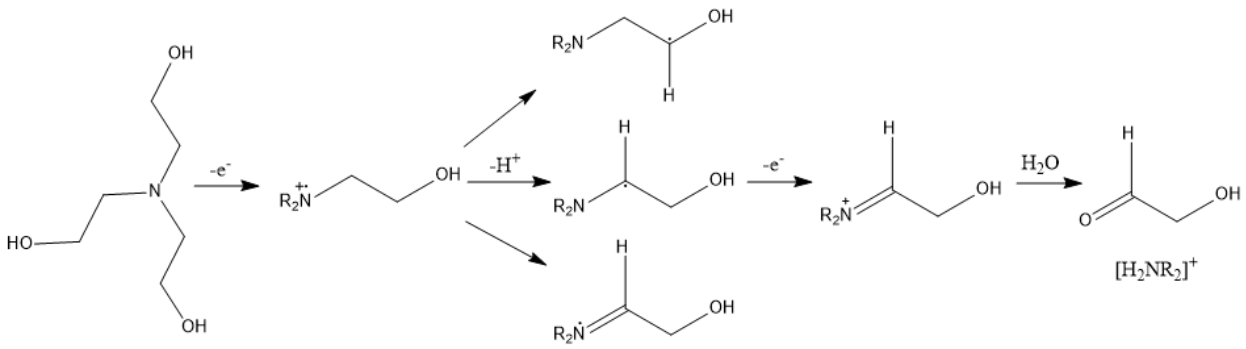

Scheme 1.3.3. Potential reactivity of the electron donor TEOA.

1.3.4 Photosensitizer (PS)

The photosensitizer is responsible for absorbing the incident light, and generating an excited state species PS*, which provides the energy to produce a chemical transformation. The electron transfer process can proceed via two different routes. The first is reductive quenching of the PS* to produce PS^{-}, and the second is oxidative quenching of the PS* to form PS^{+}. Reductive quenching occurs when the excited state photosensitizer PS* is reduced by electrons from the ED to generate a reduced compound PS^{-}. The electron is then transferred from PS^{-} to the catalyst. This reductive quenching method is the more often seen method with photocatalytic CO_2 reduction. Oxidative quenching occurs when the excited state photosensitizer (PS*) undergoes oxidative quenching by reacting with the catalyst. This

generates a reduced catalyst (Cat^{-}) and an oxidized photosensitizer (PS^{+}). The PS^{+} can be reduced by the ED to reform PS. Both oxidative and reductive quenching processes are shown in Scheme 1.3.4.1.[3,7,15]

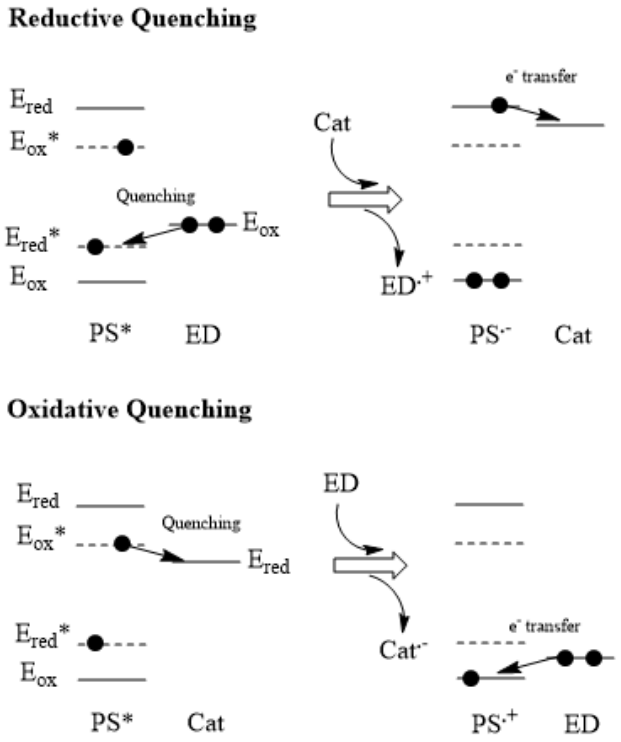

Scheme 1.3.4.1. Reductive and oxidative quenching processes.[3]

There are several factors to consider when deciding on a good photosensitizer[3,15]:

1. The PS should have a strong absorption of light, preferably in the visible region. Its absorption should be stronger at the excitation wavelength than the other components, such as the Cat and ED.
2. The PS should have a long lasting reactive excited state.
3. The PS should have high stability of the one electron reduced species.
4. The PS should have strong oxidation power of its excited state, in order to capture an electron from the reductant.

Along with the above criteria, the PS should not form ground- state complexes with the quencher and its redox potentials should also be compatible with electron transfer. The energy of the exciting photon must be sufficient to increase the oxidizing or reducing capacity of the PS. If the singlet or triplet state energy of the PS exceeds the electronic energies of the quencher, energy transfer may become competitive. The PS should therefore absorb at longer wavelengths than the quencher, while maintaining its oxidizing or reducing capacity.[15]

Tris(2,2'-bipyridine) ruthenium (II) (Figure 1.3.4) is one of the most commonly used photosensitizers. It is so commonly used because of its redox properties, chemical stability, excited state reactivity, and excited state lifetime.[2,16,17] It has an absorption at 452nm (visible region), a stable, long-lived excited state of 1100ns, and is an effective excited state oxidant and reductant. Although it is a poor single-electron oxidant and reductant in the ground state, excitation of an electron affords an excited state that is an excellent single electron transfer reagent. Upon absorption of a photon in the visible region, an electron is excited from one of the PS's metal-centered t_{2g} orbitals to a ligand-centered π^* orbital. This is a metal to ligand charge transfer (MLCT), and results in a species in which the metal has effectively been oxidized to a Ru(III) oxidation state and the ligand framework has undergone a single electron reduction. Rapid intersystem crossing (ISC) causes the initially occupied singlet MLCT state to give the lowest-energy triplet MLCT state. This triplet state is the long lived photoexcited species that engages in single electron transfer. Decay to the singlet ground state is spin-forbidden, which is the reason for its long lifetime. This photoexcited species is both more oxidizing and more reducing than the ground state species. This dual nature as both oxidant and reductant can be rationalized with the molecular orbital diagram, Scheme 1.3.4.2. The photoexcitation of $Ru(bpy)_3^{2+}$ generates a high energy electron which may be expelled from the π^* orbital when the PS acts as a reductant. Simultaneously, photoexcitation reveals a lower energy hole in the t_2g orbital which may accept an electron when the PS

acts as an oxidant. As a result, redox transformations of $Ru(bpy)_3^{2+}$ may proceed by either oxidative or reductive quenching.[17]

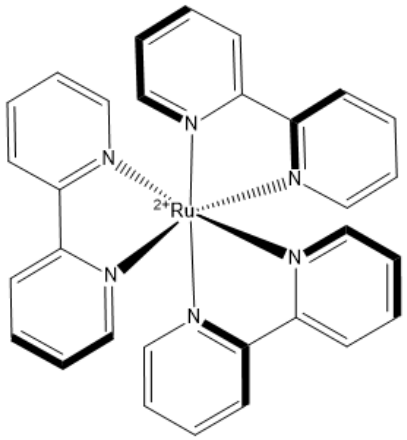

Figure 1.3.4 The structure of the Tris(2,2'-bipyridine) ruthenium (II) photosensitizer.

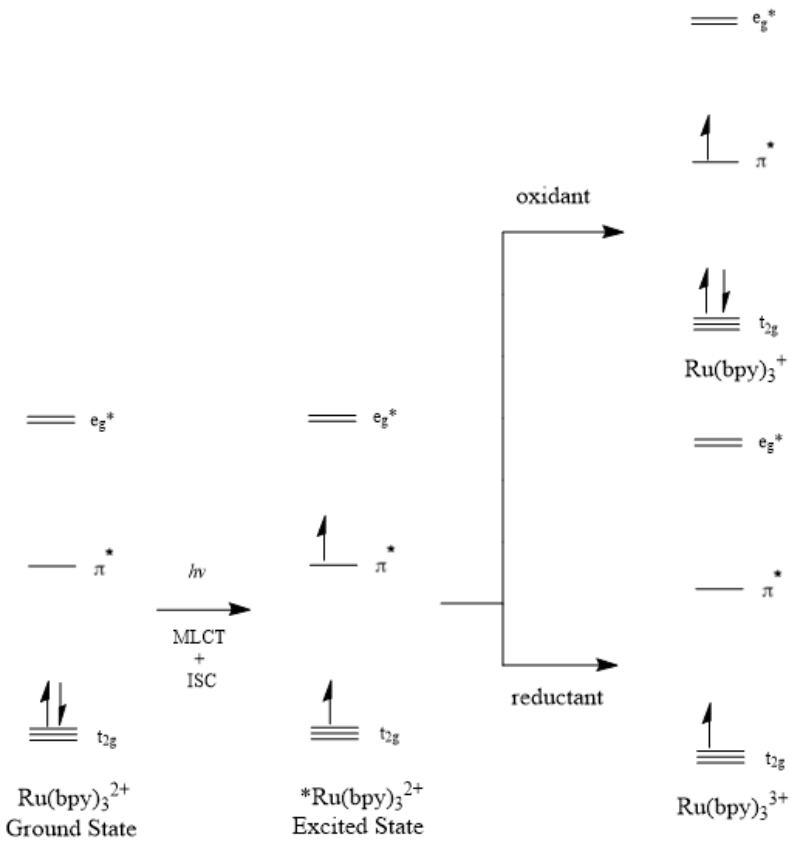

Scheme 1.3.4.2. Simplified molecular orbital depiction of $Ru(bpy)_3^{2+}$ photochemistry.[17]

1.3.5 Solvent (S)

The solvent also plays a role in a homogeneous photocatalytic system. Common solvents used in photocatalytic systems for CO_2 reduction include dimethylformamide (DMF), acetonitrile (ACN), methanol (MeOH) and dimethylacetamide (DMA). In this thesis, the solvents used in the photochemistry experiments were dimethylformamide (DMF) and dimethylacetamide (DMA).

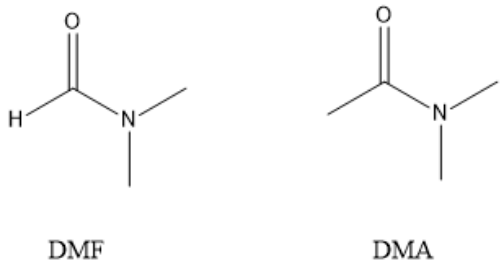

Figure 1.3.5. The structures of dimethylformamide (DMF) and dimethylacetamide (DMA).

1.3.6 Turn Over Number (TON) and Turn Over Frequency (TOF)

The turnover number is defined as the molar ratio of products to the catalyst, and is used to describe the productivity of the catalyst. It is the number of reduction processes that can occur per catalyst cycle over the catalyst's lifetime.[4] It can be defined by the equation:

$$TON = \frac{[CO_2\ Reduction\ Products]}{[Catalyst]}$$

It is an important parameter as it is a fundamental feature of a catalyst and indicates the stability of the catalyst. An 'ideal' catalyst would have an infinite TON, but real catalysts can have TON of around 1 million for industrial applications. TON for common photocatalysts studied for CO_2 reduction are often in the range of 1-500.[4]

The turn over frequency (TOF) is a related parameter which is used to describe the activity of the catalyst, which can be defined by the equation:

$$TOF = \frac{TON}{Time}$$

1.3.7 Catalytic Selectivity (CS)

In the catalytic reduction of CO_2, there are different products that can be formed, however in this thesis the focus is on formic acid/formate (HCOOH, $HCOO^-$) and carbon monoxide (CO). The catalysts used can have a selectivity for a particular reaction product. Another feature of catalytic selectivity is the selectivity of reducing equivalents. A catalyst that reduces CO_2 to products such as formate or carbon monoxide may also be able to reduce protons to hydrogen.[18] The reduction potentials of these products for the half-cell reactions at pH 7 in aqueous solution vs normal hydrogen electrode are shown in the following table. The reduction potential for hydrogen production is very similar to the reduction potentials for carbon monoxide and formic acid production, making it a competitive process.[18]

Table 1.3.7. The standard reduction potentials for half-cell reactions.[18]

Reaction	E°(V) vs SHE*
$2H^+ + 2e^- \rightarrow H_2$	-0.41 V
$CO_2 + 2H^+ + 2e^- \rightarrow CO + H_2O$	-0.52 V
$CO_2 + 2H^+ + 2e^- \rightarrow HCOOH$	-0.61 V

*E° potentials are reported at pH 7.

Catalytic selectivity also gives information about the overall efficiency of a CO_2 reduction system. There is selectivity in which CO_2 reduction products are formed, either formate or carbon monoxide. There is also the selectivity of reducing equivalents, which compares the carbon dioxide reduction products

formed to H_2 formed. It is the ratio of the moles of CO_2 reduction products to the moles of H_2. This type of catalytic selectivity can be expressed as:

$$CS = \frac{[CO_2 \text{ reduction products}]}{[H_2]}$$

This parameter is often used to quantify the efficiency of catalytic CO_2 reduction processes.[4]

1.3.8 Photochemical Quantum Yield (φ)

The photochemical quantum yield is the molar ratio of CO_2 reduction products to the incident photons.[4] It is a parameter that is used to describe the efficiency of the catalytic CO_2 reduction system. It can be expressed by the following equation.

$$\phi = \frac{[CO_2\ Reduction\ Products]}{[Incident\ Photons]}$$

This parameter is important because it normalizes results using different light sources. The number of photons absorbed by the system during a given time period must be measured in order to determine the quantum yield. The incident photon flux can be measured using chemical or physical means, such as actinometry, which is able to measure the number of photons in a beam integrally or per unit time.[19]

1.3.9 Basic Mechanism of Photocatalytic Reactions

Photocatalytic processes generally follow the same basic steps which will be outlined below. The initial steps of the photocatalytic process can be expressed using the following equations:

$$PS + h\upsilon \rightarrow PS(S1)^*$$

$$PS(S1)^* \rightarrow PS(T1)^*$$

$$PS(T1)^* + Q \rightarrow Q^- + PS^+$$

Or

$$PS(T1)^{*} + Q \rightarrow Q^{+} + PS^{-}$$

Where PS is the photosensitizer, PS* is the excited photosensitizer species, Q is the quenching molecule, S1 is a singlet state, and T1 is the triplet state.

The photocatalytic process begins with the photosensitizer, when exposed to light, absorbing a photon which is excited from the ground state (S0) to the first singlet excited state (S1). Intersystem crossing (ISC) can then occur from the singlet excited state (S1) to a longer lived triplet excited state (T1). For metal complexes, metal to ligand charge transfer may occur and the system undergoes intersystem crossing to a longer lived triplet state, so that the excited photosensitizer has more time to react with other molecules. Intersystem crossing is more probable when the vibrational levels of 2 excited states overlap, with high atomic d^6 metal centers such as Ru(II) having more intense spin-orbit coupling, and therefore intersystem crossing is more favoured. The energy is then transferred from the triplet state (T1) of the photosensitizer molecule to a quenching molecule, and the photosensitizer will undergo electron transfer to either end up as the oxidized species (PS^{+}) or the reduced species (PS^{-}).[4,7,20,21] Since reductive quenching is more common for carbon dioxide reduction, the next steps will be shown for reductive quenching.

$$PS^{-} + Cat \rightarrow PS + Cat^{-}$$

The reduced excited state photosensitizer then reacts with the catalyst, producing PS and the reduced catalyst, Cat^{-}. The reduced Cat (Cat^{-}) can then react with the CO_2 in order to form CO_2 reduction products.[4]

$$Cat^{-} + CO_2 \rightarrow Cat + Products$$

References

1. S. Nahar, M. Zain, A. Kadhum, H. Hasan and M. Hasan. Advances in Photocatalytic CO_2 Reduction with Water: A Review. *Materials (Basel)*., **2017**, 10, 629.

2. J. Wu, Y. Huang, W. Ye and Y. Li. CO_2 Reduction: From the Electrochemical to Photochemical Approach. *Adv. Sci.*, **2017**, 4, 1700194.

3. Y. Yamazaki, H. Takeda and O. Ishitani. Photocatalytic reduction of CO2 using metal complexes. *J. Photochem. Photobiol. C Photochem. Rev*., **2015**, 25, 106–137.

4. A. J. Morris, G. J. Meyer and E. Fujita. Molecular Approaches to the Photocatalytic Reduction of Carbon Dioxide for Solar Fuels. *Acc. Chem. Res*., **2009**, 42, 1983–1994.

5. J. Hong, W. Zhang, J. Ren and R. Xu. Photocatalytic reduction of CO_2: a brief review on product analysis and systematic methods. *Anal. methods*, **2013**, 5, 1086–1097.

6. A. H. A. Tinnemans, T. P. M. Koster, D. Thewissen and A. Mackor. Tetraaza-macrocyclic cobalt(II) and nickel(II) complexes as electron-transfer agents in the photo(e1ectro)chemical and electrochemical reduction of carbon dioxide. *Recl. Des Trav. Chim. des Pays-Bas*, **1984**, 103, 288–295.

7. Hiroyuki Takeda, Claudio Cometto, Osamu Ishitani, and Marc Robert. Electrons, Photons, Protons and Earth-Abundant Metal Complexes for Molecular Catalysis of CO_2 Reduction. *ACS Catal.* **2017**, 7, 70-88.

8. H. Takeda, H. Koizumi, K. Okamoto and O. Ishitani. Photocatalytic CO_2 reduction using a Mn complex as a catalyst. *Chem. Commun*., **2014**, 50, 1491–1493.

9. J. Hawecker, J.-M. Lehn and R. Ziessel. Efficient Photochemical Reduction of CO_2 to CO by Visible Light Irradiation of Systems containing $Re(bipy)(CO)_3X$ or $Ru(bipy)_3^{2+}$-Co^{2+} Combinations as Homogeneous Catalysts. *J. Chem. Soc. Chem. Commun*., **1983**, 536–538.

10. J. Hawecker, J. Lehn and R. Ziessel. Photochemical and Electrochemical Reduction of Carbon Dioxide to Carbon Monoxide Mediated by (2,2'-Bipyridine)tricarbonylchlororhenium(I) and Related Complexes as Homogeneous Catalysts). *Helv. Chim. Acta*, **1986**, 69, 1990–2012.

11. J. Grodkowski, P. Neta, E. Fujita, A. Mahammed, L. Simkhovich and Z. Gross. Reduction of Cobalt and Iron Corroles and Catalyzed Reduction of CO_2. *J. Phys. Chem. A*, **2002**, 106, 4772–4778.

12. J. Grodkowski, T. Dhanasekaran, P. Neta, P. Hambright, B. S. Brunschwig, K. Shinozaki and E. Fujita. Reduction of Cobalt and Iron Phthalocyanines and the Role of the Reduced Species in Catalyzed Photoreduction of CO_2. *J. Phys. Chem. A*, **2000**, 104, 11332–11339.

13. T Dhanasekaran, J. Grodkowski, P. Neta, P. Hambright, and Etsuko Fujita. p-Terphenyl-Sensitized Photoreduction of CO_2 with Cobalt and Iron Porphyrins. Interaction between CO and Reduced Metalloporphyrins. *J. Phys. Chem. A*, **1999**, 103, 7742–7748.

14. M. Bourrez, F. Molton, S. Chardon-Noblat and A. Deronzier. [Mn(bipyridyl)$(CO)_3$Br]: An Abundant Metal Carbonyl Complex as Efficient Electrocatalyst for CO_2 Reduction. *Angew. Chemie Int. Ed.*, **2011**, 50, 9903–9906.

15. G. J. Kavarnos and N. J. Turro. Photosensitization by Reversible Electron Transfer: Theories, Experimental Evidence, and Examples. *Chem. Rev*., **1986**, 86, 401–449.

16. Rensmo, H., Lunell, S., Siegbahn, H. Absorption and electrochemical properties of ruthenium(II) dyes, studied by semiempirical quantum chemical calculations. *J. Photochem. Photobiol. A Chem*, **1998**, 114, 117-124.

17. C. K. Prier, D. A. Rankic and D. W. C. MacMillan. Visible Light Photoredox Catalysis with Transition Metal Complexes: Applications in Organic Synthesis. *Chem. Rev*., **2013**, 113, 5322–5363.

18. J.-M. Lehn and R. Ziessel. Photochemical generation of carbon monoxide and hydrogen by reduction of carbon dioxide and water under visible light irradiation. *Proc. Natl. Acad. Sci*., **1982**, 79, 701–704.

19. S. P. Pitre, C. D. McTiernan, W. Vine, R. DiPucchio, M. Grenier and J. C. Scaiano. Visible-Light Actinometry and Intermittent Illumination as Convenient Tools to Study Ru$(bpy)_3Cl_2$ Mediated Photoredox Transformations. *Sci. Rep*., **2015**, 5, 16397.

20. R. Reithmeier, C. Bruckmeier and B. Rieger. Conversion of CO_2 via Visible Light Promoted Homogeneous Redox Catalysis. *Catalysts,* **2012**, 2, 544–571.

21. A. H. Dwivedi and U. C. Pande. Photochemical Degradation of Halogenated Compounds: A Review. *Sci. Revs. Chem. Commun*, **2012**, 2, 41–65.

22. N. Elgrishi, M. B. Chambers, X. Wang and M. Fontecave. Molecular polypyridine-based metal complexes as catalysts for the reduction of CO_2. *Chem. Soc. Rev*., **2017**, 46, 761–796.

Chapter 2: Synthesis and Characterization of Phosphinoaminopyridine Ligands and Associated Rhenium and Manganese Compounds

Reagents and analytical grade solvents were purchased from Strem Chemicals or Sigma Aldrich and used without further purification. The ^{1}HNMR spectra were recorded at 400 MHz with chemical shifts reported in ppm using the residual protons of the NMR solvent as internal standards.

2.1 Synthesis and characterization of $(Ph_2P)NMe(NC_5H_4)$ Ligand

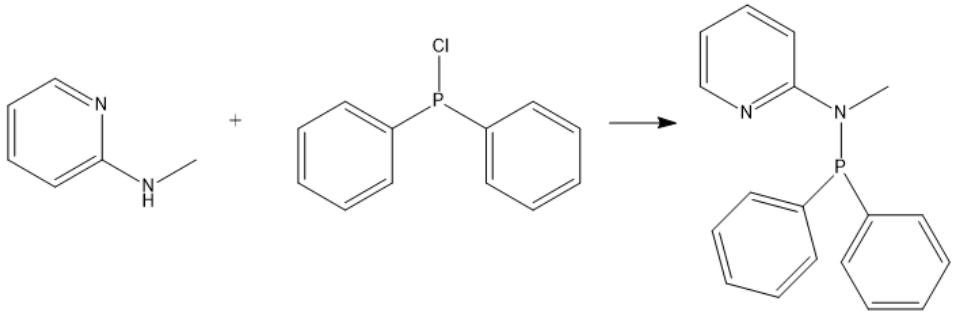

Scheme 2.1. Reaction scheme for $(Ph_2P)NMe(NC_5H_4)$ ligand.

This ligand was synthesized following literature procedure.[1] A solution of 1.08g (10.0 mmol) of 2-(methylamino)pyridine in 25mL diethyl ether was cooled to -78^{o}C using a dry ice/acetone bath. n-BuLi (10mmol, 1.6 M in hexane, 6.25mL) was added dropwise and the solution was stirred for 2 hours. A solution of PPh_2Cl (10mmol, 2.2g) in 10mL diethyl ether was added dropwise and the solution was allowed to warm to room temperature. The reaction mixture was stirred overnight. The reaction mixture was filtered twice and the solvent was removed to give an off-white solid. Yield: 2.01g (68.8%). HNMR (400 MHz, $CDCl_3$, 25^{o}C): δ= 8.25-8.30 (1H, m), 7.39-7.55 (12H, m), 6.75-6.79 (1H, m), 2.95 (3H, d)

2.2 Synthesis and characterization of κ^2-$(Ph_2P)NMe(NC_5H_4)Re(CO)_3Br$ (Catalyst 1)

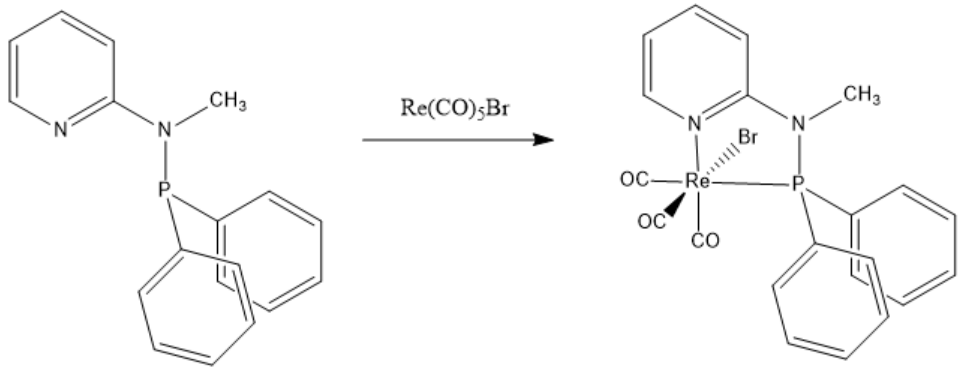

Scheme 2.2. Reaction scheme for the κ^2-$(Ph_2P)NMe(NC_5H_4)Re(CO)_3Br$ complex.

This complex was synthesized using a procedure similar to that of a literature procedure for the manganese analogue.[2] In a glovebox, a solution of $(Ph_2P)NMe(NC_5H_4)$ ligand (0.146g, 0.5mmol) was prepared in 15mL of tetrahydrofuran. $Re(CO)_5Br$ (0.203g, 0.5mmol) was added via stirring to the THF solution. The flask was wrapped in aluminum foil, removed from glovebox and connected to a Schlenk line via a reflux condenser. The reaction was heated to 100ºC under N_2 and stirred for an additional 3 hours. The solution was cooled and the volume was reduced to ~3mL and 50mL of hexanes was added to get the complex as a pinkish-white solid. HNMR (400 MHz, $CDCl_3$, 25ºC): δ= 8.76 (1H, dd), 7.76-7.83 (2H, m), 7.47-7.55 (10H, m), 6.84-6.88 (1H, m), 3.07 (3H, d). Single crystals were grown by slow diffusion of hexanes and THF (Figure 2.2). EI mass spectrometry was also performed and showed accurate mass on loss of 2 COs, with an m/z peak at 586 (73.29%).

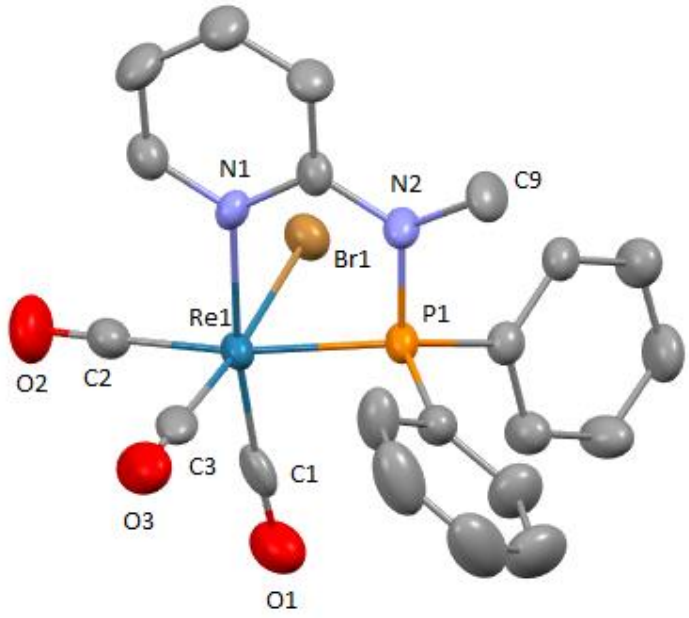

Figure 2.2. Structural representation of κ^2-$(Ph_2P)NMe(NC_5H_4)Re(CO)_3Br$ obtained from X-ray analysis, displayed with ellipsoid style. Hydrogen atoms are omitted for clarity. This structure has not been previously reported.

Table 2.2.1. Crystallographic Collection Data for κ^2-$(Ph_2P)NMe(NC_5H_4)Re(CO)_3Br$

empirical formula	$C_{21}H_{17}BrN_2O_3PRe$
formula weight ($g \cdot mol^{-1}$)	642.45
crystal system	monoclinic
space group	$P\,2_1$
a (A)	8.3671(8)
b (A)	11.2998(12)
c (A)	11.8539(11)
α (deg)	90
β (deg)	108.611(5)
γ (deg)	90
V (A^3)	1062.14(18)
Z	2

T (K)	204(2)
ρ_{calcd} (g·cm^{-3})	2.009
μ (mm^{-1})	7.701
$2\theta_{max}$ (deg)	50.046
total/unique reflections	15516/3300
Reflections [$I_o \geq 2\sigma(I_o)$]	3224
R_1, wR_2 [$I_o \geq 2\sigma(I_o)$]	0.0225, 0.0554
goodness of fit	1.053

Table 2.2.2. Selected Crystallographic Bond Lengths for κ^2-(Ph_2P)NMe(NC_5H_4)Re($CO)_3$Br. Full data set may be found in Appendix A.

Atom	Atom	Length (Å)
Re1	C1	1.880(8)
Re1	C2	1.932(9)
Re1	C3	1.959(10)
Re1	N1	2.199(5)
Re1	P1	2.404(2)
Re1	Br1	2.6143(9)
P1	N2	1.702(6)
P1	C16	1.813(8)
P1	C10	1.817(8)
O1	C1	1.195(10)
O2	C2	1.185(11)
O3	C3	1.056(11)
N1	C8	1.348(12)
N1	C4	1.349(12)
N2	C8	1.377(10)
N2	C9	1.486(11)

Table 2.2.3. Selected Crystallographic Bond Angles for κ^2-$(Ph_2P)NMe(NC_5H_4)Re(CO)_3Br$. Full data set may be found in Appendix A.

Atom	Atom	Atom	Angle (˚)
C1	Re1	C2	89.2(4)
C1	Re1	C3	90.8(3)
C2	Re1	C3	90.3(4)
C1	Re1	N1	173.1(5)
C2	Re1	N1	97.1(3)
C3	Re1	N1	92.0(3)
C1	Re1	P1	95.9(3)
C2	Re1	P1	171.9(2)
C3	Re1	P1	95.9(3)
N1	Re1	P1	77.5(3)
C1	Re1	Br1	94.4(3)
C2	Re1	Br1	87.1(3)
C3	Re1	Br1	174.2(2)
N1	Re1	Br1	83.2(2)
P1	Re1	Br1	86.29(6)

The Re(I) starting material used in this synthesis was $Re(CO)_5Br$. The direct reaction of $Re(CO)_5Br$ with the $(Ph_2P)NMe(NC_5H_4)$ ligand yielded the d^6 Re(I) complex κ^2-$(Ph_2P)NMe(NC_5H_4)Re(CO)_3Br$. Analyzing the crystal structure, it can be seen that the complex is pseudo-octahedral. There is elongation of the Re-Br bond (2.6143Å) compared to the Re-P bond (2.404Å), Re-N bond (2.199Å) and the Re-C bonds (1.880 Å, 1.932 Å, 1.959 Å). (Table 2.2.2) This pseudo-octahedral shape can also be observed when comparing the bond angles (Table 2.2.3). The angle between Br1, Re1, and C3 is 174.2°, the angle between P1, Re1, and C2 is 171.9°, and the angle between N1, Re1, and C1 is 173.1°. These bond angles differ from the expected 180° for a perfect octahedral. The structure has an N_{py}-Re-P bite angle of 77.5°. The crystal structure shows a facial (fac) isomer, with the halide (Br) trans to a CO ligand. CO is a strong field ligand, and this complex is d^6, meaning that it is likely diamagnetic. This is furthered by the fact that rhenium is

a third row transition metal, which also favours low spin compounds. Similar signals to that of the $(Ph_2P)NMe(NC_5H_4)$ ligand (Section 2.1) were found, including signals for the 10 phenyl hydrogens between 7.47-7.55 and a doublet at 3.07 for the N-Me hydrogens. Additionally, an electron impact mass spectrometry experiment was done on this complex. The molar mass of the compound is 642.45g/mol. There was a significant peak at 586m/z, corresponding to the complex on loss of 2 CO ligands (73.29%).

2.3 Synthesis and characterization of κ^2-$(Ph_2P)NMe(NC_5H_4)Re(CO)_3OTf$

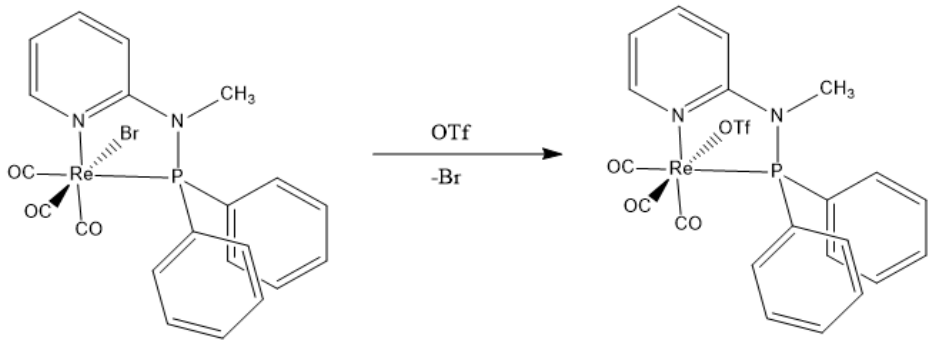

Scheme 2.3 Reaction scheme for the κ^2-$(Ph_2P)NMe(NC_5H_4)Re(CO)_3OTf$ complex.

This complex was synthesized using a procedure similar to that of a literature procedure for the manganese analogue.[2] 0.032g (0.5mmol) of κ-$(Ph_2P)NMe(NC_5H_4)Re(CO)_3Br$ was dissolved in a 1:1 solution of toluene: DCM (10mL: 10mL). A solution of silver trifluoromethanesulfonate (0.128g, 0.5mmol) was made in 20mL of DCM. The κ-$(Ph_2P)NMe(NC_5H_4)Re(CO)_3Br$ solution was then added to the silver solution and the flask was wrapped in aluminum foil, and connected to a Schlenk line via a reflux condenser. The reaction was stirred for 2 hours under N_2 at room temperature. AgBr precipitate was removed by filtration through a syringe filter, and the solvent was removed to give a dark purple solid and colourless needle- like crystals. This procedure was followed several times, and each time yielded the same result. Colourless needle-like crystals were submitted for single crystal X-ray analysis but

returned the crystal structure of $[Re(CO)_x(OTf)_y]_z$, which did not contain the desired ligand. Additionally, the ^{1}HNMR spectrum did not show any desired peaks.

2.4 Synthesis and characterization of κ^2-$(Ph_2P)NMe(NC_5H_4)Re(CO)_3Cl$

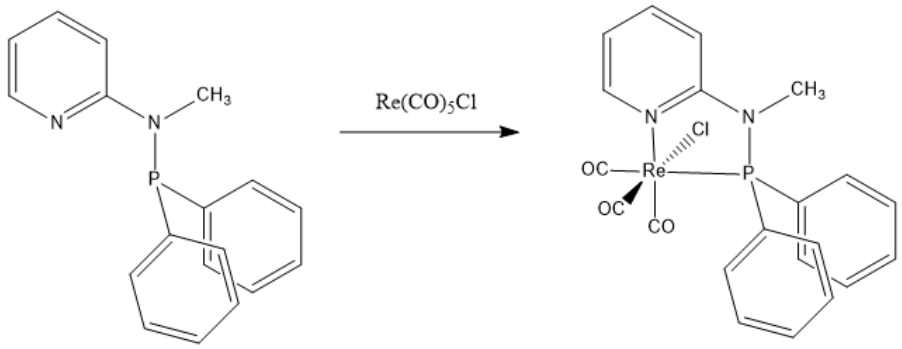

Scheme 2.4 Reaction scheme for the κ^2-$(Ph_2P)NMe(NC_5H_4)Re(CO)_3Cl$ complex.

This complex was synthesized using a procedure similar to that of a literature procedure for the manganese analogue.[2] In a glovebox, a solution of $(Ph_2P)NMe(NC_5H_4)$ ligand (0.146g, 0.5mmol) was prepared in 15mL of tetrahydrofuran. $Re(CO)_5Cl$ (0.181g, 0.5mmol) was added via stirring to the THF solution. The flask was wrapped in aluminum foil, removed from glovebox and connected to a Schlenk line via a reflux condenser. The reaction was heated to 100^{o}C under N_2 and stirred for an additional 3 hours. The solution was cooled and the volume was reduced to ~3mL and 50mL of hexanes was added to get the complex as a tan-yellow solid. No crystals could be grown for single crystal X-ray analysis. Additionally, the ^{1}HNMR spectrum did not show any desired peaks.

2.5 Synthesis and characterization of ([$(CH_3)_2CH]_2$P)NMe(NC_5H_4) Ligand

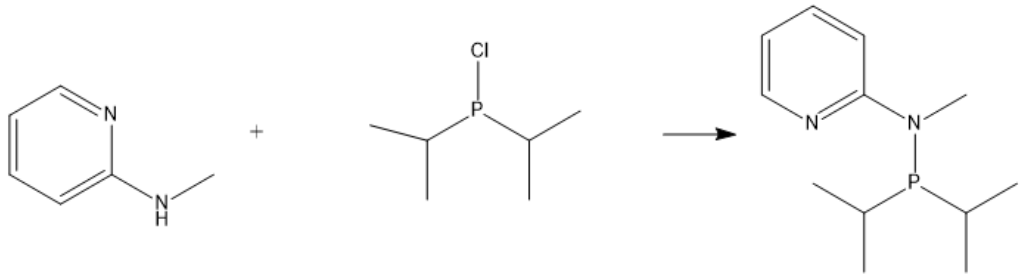

Scheme 2.5. Reaction scheme for ([$(CH_3)_2CH]_2$P)NMe(NC_5H_4) ligand.

This ligand was synthesized using a modified literature procedure.[3] A solution of 1.08g (10.0 mmol) of 2-(methylamino)pyridine in 30mL diethyl ether was cooled to -78°C using a dry ice/acetone bath. n-BuLi (10mmol, 1.6 M in hexane, 6.25mL) was added dropwise and the solution was stirred for 3 hours. A solution of $[(CH_3)_2CH]_2PCl$ (10mmol, 1.534g) was added dropwise and the solution was allowed to warm to room temperature. The reaction mixture was stirred overnight. The reaction mixture was filtered twice and washed with diethyl ether, and the solvent was removed to give a yellow oil. Yield: 1.64g (73.1%). HNMR (400 MHz, $CDCl_3$, 25°C): δ= 8.14 (1H, d), 7.36-7.5 (2H, m), 6.58 (1H, t), 3.02 (3H, d), 2.06-2.15 (2H, m), 1.09 (6H, q), 0.98 (6H, q)

2.6 Synthesis and characterization of κ^2-([$(CH_3)_2CH]_2$P)NMe(NC_5H_4)Re$(CO)_3$Br (Catalyst 2)

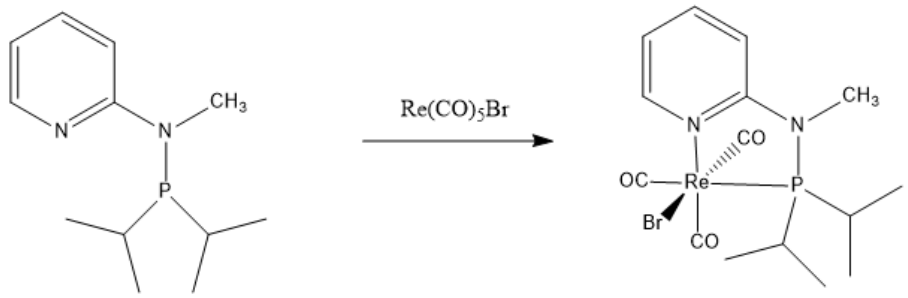

Scheme 2.6. Reaction scheme for the κ^2-([$(CH_3)_2CH]_2$P)NMe(NC_5H_4)Re$(CO)_3$Br complex.

In a glovebox, a solution of ([$(CH_3)_2CH]_2$P)NMe(NC_5H_4) ligand (0.112g, 0.5mmol) was prepared in 15mL of tetrahydrofuran. $Re(CO)_5Br$ (0.203g, 0.5mmol) was added via stirring to the THF solution. The flask was wrapped in aluminum foil, removed from the glovebox and connected to a Schlenk line via a reflux condenser. The reaction was heated to 100^{0}C under N_2 and stirred for an additional 3 hours. The solution was cooled and the volume was reduced to ~3mL and 50mL of hexanes was added to get the complex as a pinkish-white solid. HNMR (400 MHz, $CDCl_3$, 25^{0}C): δ= 8.69 (1H, dd), 7.67-7.72 (1H, m), 6.7-6.77 (2H, m), 3.10 (3H, d), 2.85-2.95 (1H, m), 2.62- 2.73 (1H, m), 1.36-1.5 (10H, m), 1.11 (2H, q). Single crystals were grown by slow diffusion of pentane and DCM (Figure 2.6).

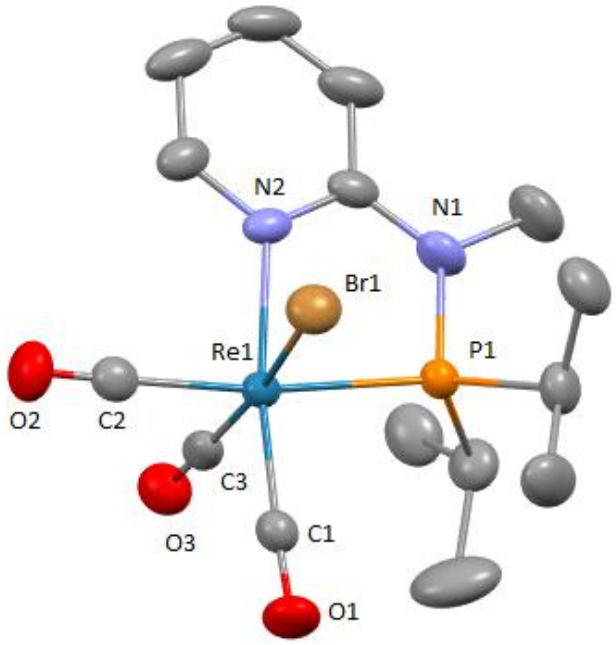

Figure 2.6. Structural representation of κ^2-([$(CH_3)_2CH]_2$P)NMe(NC_5H_4)Re($CO)_3$Br obtained from X-ray analysis, displayed with ellipsoid style. Hydrogen atoms are omitted for clarity. This structure has not been previously reported.

Table 2.6.1. Crystallographic Collection Data for κ^2-([$(CH_3)_2CH]_2$P)NMe(NC_5H_4)Re($CO)_3$Br.

empirical formula	$C_{15}H_{21}BrN_2O_3PRe$
formula weight ($g \cdot mol^{-1}$)	574.42
crystal system	monoclinic
space group	$P\,2_1/c$
a (A)	11.161(6)
b (A)	13.350(8)
c (A)	12.448(7)
α (deg)	90
β (deg)	96.315(11)
γ (deg)	90
V (A^3)	1843.5(18)
Z	4
T (K)	203(2)

ρ_{calcd} (g·cm^{-3})	2.070
μ (mm^{-1})	8.860
$2\theta_{max}$ (deg)	73.286
total/unique reflections	48500/9053
Reflections [$I_o \geq 2\sigma(I_o)$]	6443
R_1, wR_2 [$I_o \geq 2\sigma(I_o)$]	0.0349, 0.0623
goodness of fit	1.046

Table 2.6.2. Selected Crystallographic Bond Lengths for κ^2-([$(CH_3)_2CH]_2$P)NMe(NC_5H_4)Re($CO)_3$Br. Full data set may be found in Appendix B.

Atom	**Atom**	**Length (Å)**
Re1	C1	1.919(3)
Re1	C3	1.923(4)
Re1	C2	1.971(4)
Re1	N2	2.202(3)
Re1	P1	2.4237(15)
Re1	Br1	2.6427(13)
P1	N1	1.712(3)
P1	C7	1.850(4)
P1	C4	1.862(3)
O1	C1	1.153(4)
O2	C2	1.132(4)
O3	C3	1.093(4)
N1	C11	1.379(4)
N1	C10	1.478(4)
N2	C11	1.360(4)
N2	C15	1.361(4)

Table 2.6.3. Selected Crystallographic Bond Angles for κ^2-([$(CH_3)_2CH]_2$P)NMe(NC_5H_4)Re$(CO)_3$Br. Full data set may be found in Appendix B.

Atom	Atom	Atom	Angle (˚)
C1	Re1	C3	88.33(14)
C1	Re1	C2	92.18(13)
C3	Re1	C2	87.82(13)
C1	Re1	N2	171.91(11)
C3	Re1	N2	95.15(12)
C2	Re1	N2	95.25(12)
C1	Re1	P1	94.87(10)
C3	Re1	P1	93.91(9)
C2	Re1	P1	172.79(10)
N2	Re1	P1	77.63(8)
C1	Re1	Br1	90.62(10)
C3	Re1	Br1	171.98(9)
C2	Re1	Br1	84.27(9)
N2	Re1	Br1	86.93(7)
P1	Re1	Br1	94.11(2)

The complex κ^2-([$(CH_3)_2CH]_2$P)NMe(NC_5H_4)Re$(CO)_3$Br was targeted as a means to investigate the effect that changing the substituents on the phosphorus atom and their role in the reactivity of this complex. In all of the previous work, only phenyl substituents on the phosphorus atom had been explored. The $Re(CO)_5Br$ starting material is Re(I), and reacting with the ([$(CH_3)_2CH]_2$P)NMe(NC_5H_4) ligand gives a complex that is also a d^6 Re(I) complex. Examining the crystal structure, the complex is pseudo-octahedral. There is elongation of the Re-Br bond (2.643Å) compared to the Re-P bond (2.424Å), Re-N bond (2.202Å) and the Re-C bonds (1.919 Å, 1.971 Å, 1.923 Å). (Table 2.6.2). This pseudo-octahedral shape can also be observed when comparing the bond angles (Table 2.6.3). The angle between Br1, Re1, and C3 is 171.98°, the angle between P1, Re1, and C2 is 172.79°, and the angle between N2, Re1, and C1 is 171.91°. This differs from the 180° for a perfect octahedral. The structure has an N_{py}-Re-P bite angle of

77.63°. The crystal structure shows a facial (fac) isomer, with the bromo ligand trans to a CO ligand. All of these bond lengths and bond angles are extremely similar to that of κ^2-$(Ph_2P)NMe(NC_5H_4)Re(CO)_3Br$ (Section 2.2). Since CO is a strong field ligand, and this complex is d^6, it is likely diamagnetic. This is furthered by the fact that rhenium is a third row transition metal, which also favours low spin compounds. Similar NMR signals to that of the ligand (Section 2.5) were found, including signals for the 12 isopropyl hydrogens between 1.11-1.5, and the doublet peak at 3.10 for the N-Me hydrogens.

2.7 Synthesis and characterization of κ^2-$([(CH_3)_2CH]_2P)NMe(NC_5H_4)Mn(CO)_3Br$

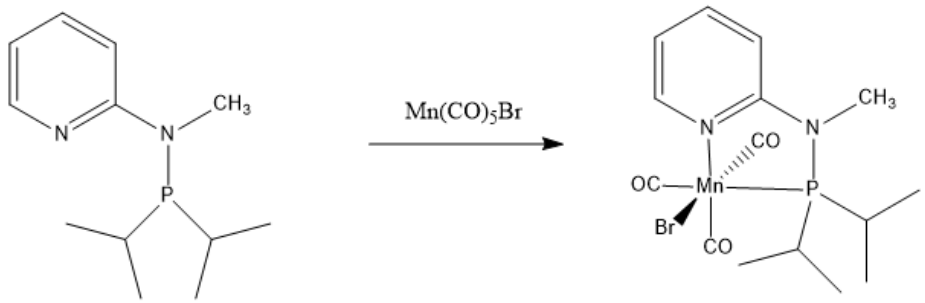

Scheme 2.7. Reaction scheme for the κ^2-$([(CH_3)_2CH]_2P)NMe(NC_5H_4)Mn(CO)_3Br$ complex.

In a glovebox, a solution of $([(CH_3)_2CH]_2P)NMe(NC_5H_4)$ ligand (0.112g, 0.5mmol) was prepared in 15mL of tetrahydrofuran. $Mn(CO)_5Br$ (0.137g, 0.5mmol) was added via stirring to the THF solution. The flask was wrapped in aluminum foil, removed from glovebox and connected to a Schlenk line via a reflux condenser. The reaction was heated to 100°C under N_2 and stirred for an additional 3 hours. The solution was cooled and the volume was reduced to ~3mL and 50mL of hexanes was added in order to precipitate out a solid product. Solution instead become clear and yellow, with no visible precipitate. Vacuum filtration was performed on the solution, however the yellow solution passed right through the filter paper. Solution was then transferred into another round-bottom flask and placed onto a rotary

evaporator. A dark yellow oil was obtained. The HNMR spectrum did not show any desired signals. Additionally no crystals could be grown for single crystal X-ray analysis.

2.8 Synthesis and Characterization of ([(CH$_3$)$_2$CH]$_2$P)NH(NC$_5$H$_4$) Ligand

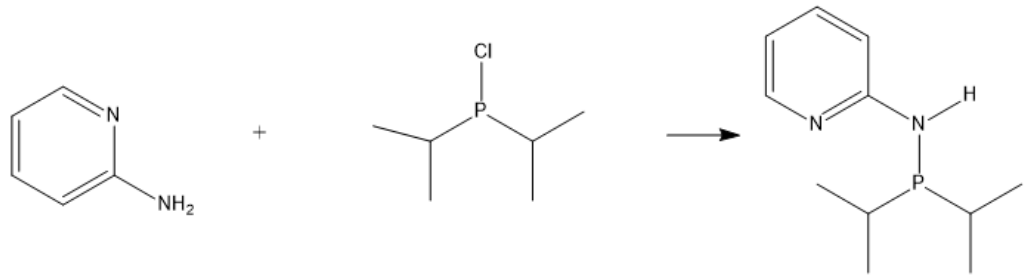

Scheme 2.8. Reaction scheme for ([(CH$_3$)$_2$CH]$_2$P)NH(NC$_5$H$_4$) ligand.

This ligand was synthesized using a modified literature procedure.[4] A solution of 0.94g (10.0 mmol) of 2-aminopyridine in 30mL diethyl ether was cooled to -78^{o}C using a dry ice/acetone bath. n-BuLi (10mmol, 1.6 M in hexane, 6.25mL) was added dropwise and the solution was stirred for 2 hours. A solution of [(CH$_3$)$_2$CH]$_2$PCl (10mmol, 1.534g) was added dropwise and the solution was allowed to warm to room temperature. The reaction mixture was stirred overnight. The reaction mixture was filtered twice and washed with diethyl ether, and the solvent was removed to give a yellow oil. Yield: 1.59g (75.6%). HNMR (400 MHz, CDCl$_3$, 25^{o}C): δ= 7.98 (1H, d), 7.42 (1H, t), 7.08 (1H, d), 6.58-6.61 (1H, m), 4.94 (1H, broad s), 1.74-1.83 (2H, m), 1.00-1.1 (12H, m)

2.9 Synthesis and characterization of κ^2-([$(CH_3)_2CH]_2$P)NH(NC_5H_4)Re$(CO)_3$Br (Catalyst 3)

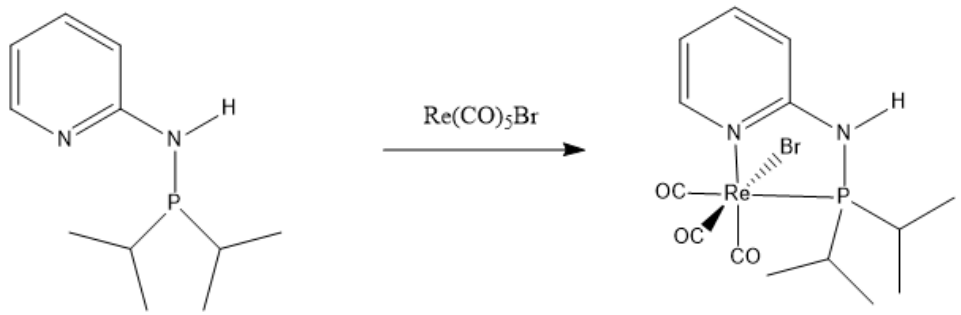

Scheme 2.9. Reaction scheme for the κ^2-([$(CH_3)_2CH]_2$P)NH(NC_5H_4)Re$(CO)_3$Br complex.

In a glovebox, a solution of ([$(CH_3)_2CH]_2$P)NH(NC_5H_4) ligand (0.105g, 0.5mmol) was prepared in 15mL of tetrahydrofuran. Re$(CO)_5$Br (0.203g, 0.5mmol) was added via stirring to the THF solution. The flask was wrapped in aluminum foil, removed from glovebox and connected to a Schlenk line via a reflux condenser. The reaction was heated to 100^{o}C under N_2 and stirred for an additional 3 hours. The solution was cooled and the volume was reduced to ~3mL and 50mL of hexanes was added to get the complex as a pinkish-white solid. HNMR (400 MHz, $CDCl_3$, 25^{o}C): δ= 8.53 (1H, td), 7.52-7.60 (1H, m), 6.91 (1H, dd), 6.64-6.71 (1H, m), 5.67 (1H, broad s), 2.52-2.62 (1H, m), 1.48 (1H, d), 1.32-1.45 (12H, m) Single crystals were grown by slow diffusion of pentane and DCM. (Figure 2.9.1).

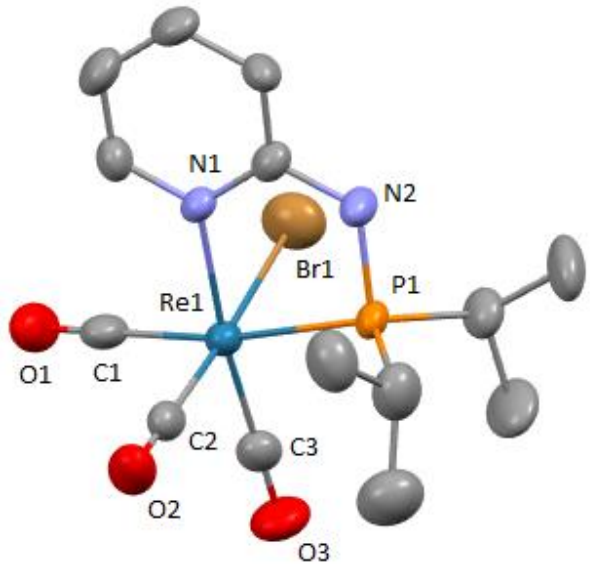

Figure 2.9.1. Structural representation of κ^2-([$(CH_3)_2CH]_2$P)NH(NC_5H_4)Re$(CO)_3$Br obtained from X-ray analysis, displayed with ellipsoid style. Hydrogen atoms are omitted for clarity. This structure has not been previously reported.

Table 2.9.1. Crystallographic Collection Data for κ^2-([$(CH_3)_2CH]_2$P)NH(NC_5H_4)Re$(CO)_3$Br

empirical formula	$C_{14}H_{18}BrN_2O_3PRe$
formula weight (g·mol^{-1})	559.38
crystal system	orthorhombic
space group	*P b c n*
a (A)	29.4722(19)
b (A)	10.0397(6)
c (A)	12.1191(7)
α (deg)	90
β (deg)	90
γ (deg)	90
V (A^3)	3585.9(4)
Z	8
T (K)	203(2)
ρ_{calcd} (g·cm^{-3})	2.072

μ (mm^{-1})	9.106
$2\theta_{max}$ (deg)	57.174
total/unique reflections	35829/4578
Reflections [$I_o \geq 2\sigma(I_o)$]	3391
R_1, wR_2 [$I_o \geq 2\sigma(I_o)$]	0.0466, 0.1301
goodness of fit	1.036

Table 2.9.2. Selected Crystallographic Bond Lengths for κ^2-([$(CH_3)_2CH]_2$P)NH(NC_5H_4)Re($CO)_3$Br. Full data set may be found in Appendix C.

Atom	Atom	Length (Å)
Re1	C2	1.921(10)
Re1	C3	1.928(9)
Re1	C1	1.962(10)
Re1	N1	2.210(6)
Re1	P1	2.430(2)
Re1	Br1	2.5833(12)
P1	N2	1.692(7)
P1	C9	1.834(9)
P1	C12	1.855(11)
N1	C4	1.351(10)
N1	C8	1.352(11)
O1	C1	1.137(11)
O3	C3	1.145(11)
C2	O2	1.118(11)
N2	C8	1.386(10)

Table 2.9.3. Selected Crystallographic Bond Angles for κ^2-([$(CH_3)_2CH]_2$P)NH(NC_5H_4)Re($CO)_3$Br. Full data set may be found in Appendix C.

Atom	Atom	Atom	Angle (˚)
C2	Re1	C3	88.0(4)

C2	Re1	C1	90.7(4)
C3	Re1	C1	90.1(4)
C2	Re1	N1	96.2(3)
C3	Re1	N1	174.1(3)
C1	Re1	N1	94.1(3)
C2	Re1	P1	95.2(3)
C3	Re1	P1	97.1(3)
C1	Re1	P1	170.9(3)
N1	Re1	P1	78.38(18)
C2	Re1	Br1	176.7(3)
C3	Re1	Br1	94.9(3)
C1	Re1	Br1	87.7(3)
N1	Re1	Br1	81.11(17)
P1	Re1	Br1	86.12(6)

This structure is analogous to that of Catalyst 2, having a hydrogen atom attached to the nitrogen instead of a methyl group. The $Re(CO)_5Br$ starting material is Re(I), and reacting with the $([(CH_3)_2CH]_2P)NH(NC_5H_4)$ ligand gives a complex that is again a d^6 Re(I) complex. Analyzing the crystal structure, the complex is pseudo-octahedral. There is elongation of the Re-Br bond (2.583Å) compared to the Re-P bond (2.430Å), Re-N bond (2.210Å) and the Re-C bonds (1.962 Å, 1.928 Å, 1.921 Å). (Table 2.9.2) This pseudo-octahedral shape can also be observed when examining the bond angles (Table 2.9.3). The angle between Br1, Re1, and C2 is 176.7°, the angle between P1, Re1, and C1 is 170.9°, and the angle between N1, Re1, and C3 is 174.1°. This differs from the expected 180° for a perfect octahedral. The structure has an N_{py}-Re-P bite angle of 78.38°. The crystal structure shows a facial (fac) isomer, with the bromo ligand trans to a CO ligand. All of these bond lengths and bond angles are extremely similar to that of κ^2-$(Ph_2P)NMe(NC_5H_4)Re(CO)_3Br$ (Section 2.2) and κ^2-$([(CH_3)_2CH]_2P)NMe(NC_5H_4)Re(CO)_3Br$ (Section 2.6). CO is a strong field ligand, and this complex is d^6, meaning it is likely diamagnetic. This is furthered by the fact that rhenium is a third row transition metal,

which also favours low spin compounds. Similar NMR signals to that of the ligand (Section 2.8) were found, including signals for the 12 isopropyl hydrogens between 1.32-1.45, and a broad singlet at 5.67 corresponding to the N-H. Additionally, the electrochemical properties of this compound were investigated. A cyclic voltammogram (Figure 2.9.2) was obtained, showing two irreversible peaks at -2.5 and -2.9 V referenced against the ferrocene/ferrocenium couple. There were some unusual observations about this cyclic voltammetry (CV) experiment. In particular, the appearance of the CV's changed on repeated scans and eventually these reduction events were no longer observed. At this point we are attributing these observations to possible chemical reactions of this complex with acetonitrile or decomposition of these reduced species. Further investigation of the electrochemical behaviour of this compound is needed.

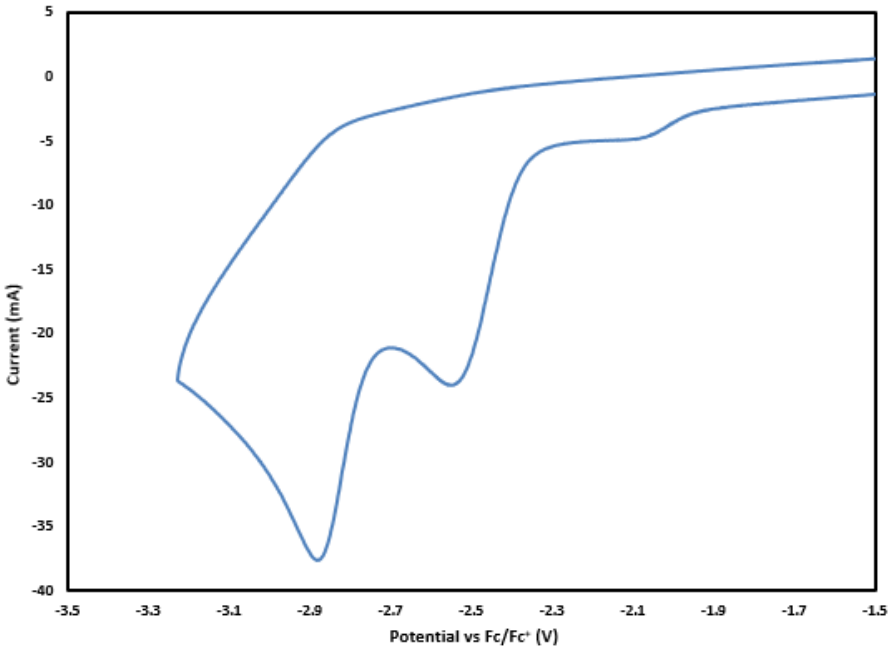

Figure 2.9.2 Cyclic voltammogram for κ^2-([$(CH_3)_2CH]_2$P)NH(NC_5H_4)Re$(CO)_3$Br in acetonitrile, corrected for ferrocene.

2.10 Synthesis and characterization of $[\kappa^2\text{-}[([(CH_3)_2CH]_2PO)NH(NC_5H_4)]_2MnBr]^{1+}$ Br^- (Catalyst 4)

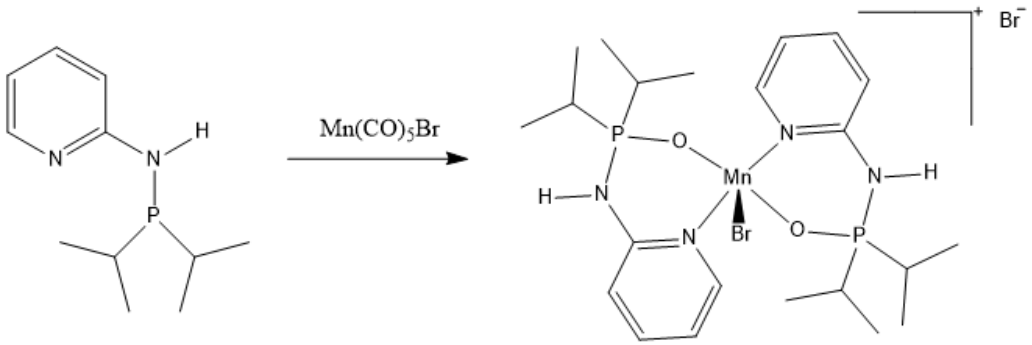

Scheme 2.10. Reaction scheme for the $[\kappa^2\text{-}[([(CH_3)_2CH]_2PO)NH(NC_5H_4)]_2MnBr]^{1+}$ Br^- compound.

In a glovebox, a solution of $([(CH_3)_2CH]_2P)NH(NC_5H_4)$ ligand (0.105g, 0.5mmol) was prepared in 15mL of tetrahydrofuran. $Mn(CO)_5Br$ (0.137g, 0.5mmol) was added via stirring to the THF solution. The flask was wrapped in aluminum foil, removed from glovebox and connected to a Schlenk line via a reflux condenser. The reaction was heated to 100^{0}C under N_2 and stirred for an additional 3 hours. The solution was cooled and the volume was reduced to ~3mL and 50mL of hexanes was added to get the complex as bright yellow solid. HNMR (400 MHz, C_2D_3N, 25^{0}C): δ= 7.71 (1H, m), 7.55 (1H, m), 6.88 (1H, t), 6.63 (1H, m), 6.57 (1H, t), 1.16 (14H, m). Single crystals were grown by slow diffusion of pentane and DCM. (Figure 2.10.1). The crystal structure was surprising, as it contained two oxidized phosphinoaminopyridine ligands, with the oxygen likely coming from exposure to the air.

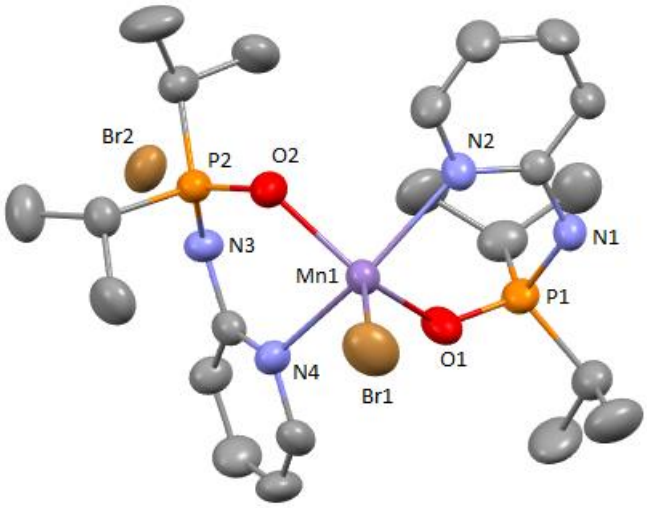

Figure 2.10.1. Structural representation of $[\kappa^2\text{-}[([(CH_3)_2CH]_2PO)NH(NC_5H_4)]_2MnBr]^{1+}$ Br^- obtained from X-ray analysis, displayed with ellipsoid style. Hydrogen atoms are omitted for clarity. This structure has not been previously reported.

Table 2.10.1. Crystallographic Collection Data for $[\kappa^2\text{-}[([(CH_3)_2CH]_2PO)NH(NC_5H_4)]_2MnBr]^{1+}$ Br^-.

empirical formula	$C_{22}H_{38}Br_2MnN_4O_2P_2$
formula weight ($g \cdot mol^{-1}$)	667.26
crystal system	monoclinic
space group	$P\,2_1$
a (A)	10.7401(4)
b (A)	11.0919(4)
c (A)	12.3824(5)
α (deg)	90
β (deg)	90.879(12)
γ (deg)	90
V (A^3)	1474.92(10)
Z	2
T (K)	203(2)
ρ_{calcd} ($g \cdot cm^{-3}$)	1.502
μ (mm^{-1})	3.290

$2\theta_{max}$ (deg)	53.036
total/unique reflections	8517/5253
Reflections [$I_o \geq 2\sigma(I_o)$]	4547
R_1, wR_2 [$I_o \geq 2\sigma(I_o)$]	0.0419, 0.1100
goodness of fit	1.052

Table 2.10.2. Selected Crystallographic Bond Lengths for $[\kappa^2\text{-}[([(CH_3)_2CH]_2PO)NH(NC_5H_4)]_2MnBr]^{1+}$ Br^-. Full data set may be found in Appendix D.

Atom	**Atom**	**Length (Å)**
Br1	Mn1	2.4378(14)
Mn1	O1	2.062(6)
Mn1	O2	2.081(5)
Mn1	N2	2.316(6)
Mn1	N4	2.321(6)
P1	O1	1.480(6)
P1	N1	1.662(6)
P1	C1	1.807(8)
P1	C4	1.810(9)
P2	O2	1.502(5)
P2	N3	1.664(6)
P2	C12	1.806(9)
P2	C15	1.810(8)
N1	C7	1.388(9)
N2	C7	1.339(9)
N2	C11	1.370(10)
N3	C18	1.392(10)
N4	C18	1.340(10)
N4	C22	1.352(10)

Table 2.10.3. Selected Crystallographic Bond Angles for $[\kappa^2\text{-}[([(CH_3)_2CH]_2PO)NH(NC_5H_4)]_2MnBr]^{1+}$ Br^-. Full data set may be found in Appendix D.

Atom	Atom	Atom	Angle (˚)
O1	Mn1	O2	135.1(2)
O1	Mn1	N2	85.7(2)
O2	Mn1	N2	89.4(2)
O1	Mn1	N4	78.8(2)
O2	Mn1	N4	85.26(19)
N2	Mn1	N4	151.7(2)
O1	Mn1	Br1	112.86(18)
O2	Mn1	Br1	111.62(17)
N2	Mn1	Br1	103.97(16)
N4	Mn1	Br1	103.87(17)

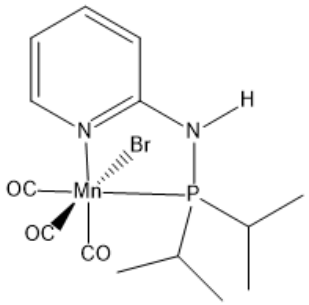

Figure 2.10.2. Initial target structure of $\kappa^2\text{-}([(CH_3)_2CH]_2P)NH(NC_5H_4)Mn(CO)_3Br$.

Crystallization of this product yielded single crystals that were analyzed by single crystal X-ray diffraction analysis. Surprisingly, the resultant structure displayed a structure with two oxidized phosphinoaminopyridine ligands attached, with the fifth coordination site filled by a bromide ligand. This crystal structure is a cation, and has a bromide counter ion. Therefore the manganese metal center is Mn(II), meaning that it is a d^5 complex. Examining the crystal structure, the complex is a square based pyramid. A d^5 square based pyramid complex is paramagnetic. The structure has N_{py}-Mn-O bite angles of

85.3° and 85.26° (Table 2.10.2). These bite angles are slightly larger than the bite angles for the un-oxidized rhenium compounds presented earlier. The Mn-Br bond distance (2.438Å) is slightly longer than the Mn-O bonds (2.062Å and 2.081Å) and the Mn-N bonds (2.316Å and 2.321Å) (Table 2.10.3). The solid product was analysed by ^{1}HNMR and electron impact mass spectrometry. The first HNMR performed in deuterated chloroform ($CDCl_3$) did not show any signals. A second HNMR done in deuterated acetonitrile (C_2D_3N) showed weak signals that are similar to that of the ligand. Electron impact mass spectrometry was performed, and several of the peaks observed could correspond to the ligand. A peak at 210m/z could correspond to the $([(CH_3)_2CH]_2P)NH(NC_5H_4)$ ligand, and a peak at 167m/z may correspond to the ligand on loss of one of the isopropyl groups. Additionally, the electrochemical properties of this compound were investigated. A cyclic voltammogram (Figure 2.10.3) was obtained, showing two irreversible peaks at -2.45 and -2.85 V referenced against the ferrocene/ferrocenium couple. There were some unusual observations about this cyclic voltammetry (CV) experiment. In particular, the appearance of the CV's changed on repeated scans and eventually these reduction events were no longer observed. At this point we are attributing these observations to possible chemical reactions of this complex with acetonitrile or decomposition of these reduced species. Further investigation of the electrochemical behaviour of this compound is needed.

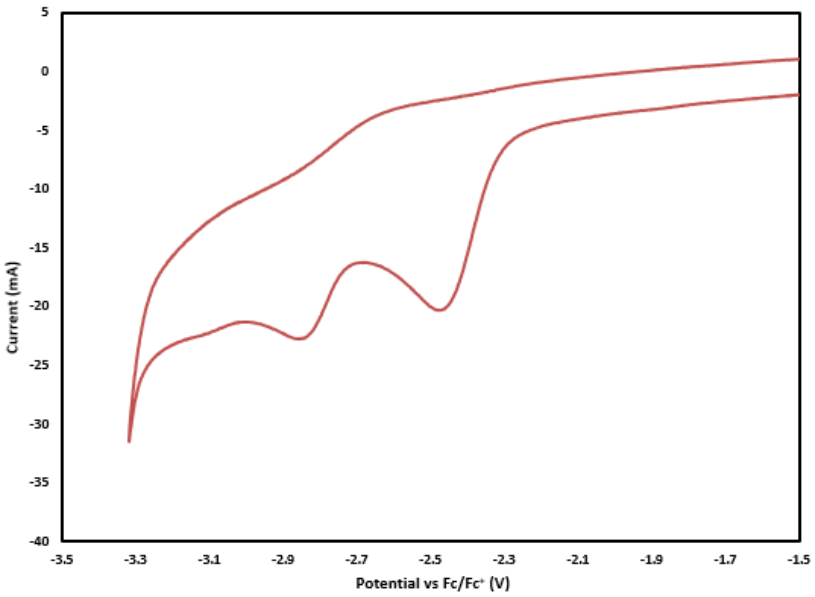

Figure 2.10.3 Cyclic voltammogram for $[\kappa^2\text{-}[([(CH_3)_2CH]_2PO)NH(NC_5H_4)]_2MnBr]^{1+}$ Br^- in acetonitrile, corrected for ferrocene.

2.11 Synthesis and characterization of $([(CH_3)_3C]_2P)NMe(NC_5H_4)$ Ligand

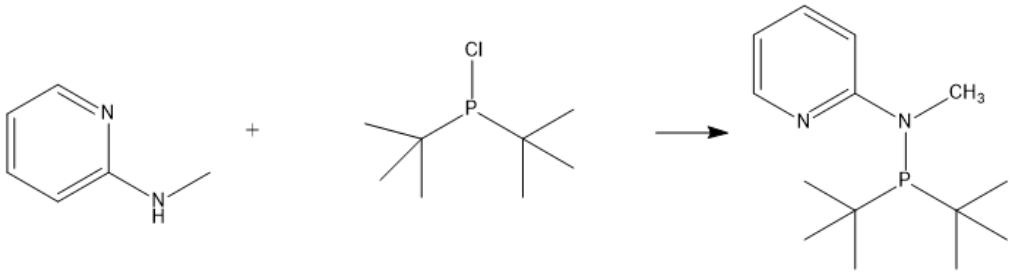

Scheme 2.11. Reaction scheme for $([(CH_3)_3C]_2P)NMe(NC_5H_4)$ ligand.

This ligand was synthesized using a modified literature procedure.[5] A solution of 1.08g (10.0 mmol) of 2-(methylamino)pyridine in 30mL diethyl ether was cooled to -78ºC using a dry ice/acetone bath. n-BuLi (10mmol, 1.6 M in hexane, 6.25mL) was added dropwise and the solution was stirred for 3 hours. A solution of $[(CH_3)_3C]_2PCl$ (10mmol, 1.806g) was added dropwise and the solution was allowed to warm to room temperature. The reaction mixture was stirred overnight. The reaction mixture was filtered

twice and washed with diethyl ether, and the solvent was removed to give an orange- yellow liquid. Yield: 1.42g (56.3%). HNMR (400 MHz, C_6D_6, 25^{o}C): δ= 8.35 (1H, d), 7.13 (1H, td), 6.36, (1H, t), 6.04 (1H, d), 2.58 (3H, s), 1.15 (18H, d)

2.12 Synthesis and characterization of κ^2-([$(CH_3)_3C]_2$P)NMe(NC_5H_4)Re$(CO)_3$

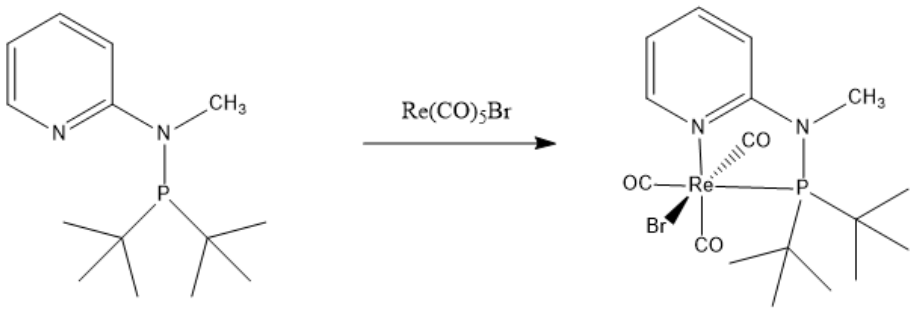

Scheme 2.12. Reaction scheme for the κ^2-([$(CH_3)_3C]_2$P)NMe(NC_5H_4)Re$(CO)_3$Br compound.

In a glovebox, a solution of ([$(CH_3)_3C]_2$P)NH(NC_5H_4) ligand (0.126g, 0.5mmol) was prepared in 15mL of tetrahydrofuran. $Re(CO)_5Br$ (0.203g, 0.5mmol) was added via stirring to the THF solution. The flask was wrapped in aluminum foil, removed from glovebox and connected to a Schlenk line via a reflux condenser. The reaction was heated to 100^{o}C under N_2 and stirred for an additional 3 hours. The solution was cooled and the volume was reduced to ~3mL and 50mL of hexanes was added to get the complex as a sticky brown solid. The HNMR spectrum gave no desired signals. No crystals could be grown for single crystal analysis.

2.13 Synthesis and characterization of κ^2-([$(CH_3)_3C]_2$P)NMe(NC_5H_4)Mn$(CO)_3$

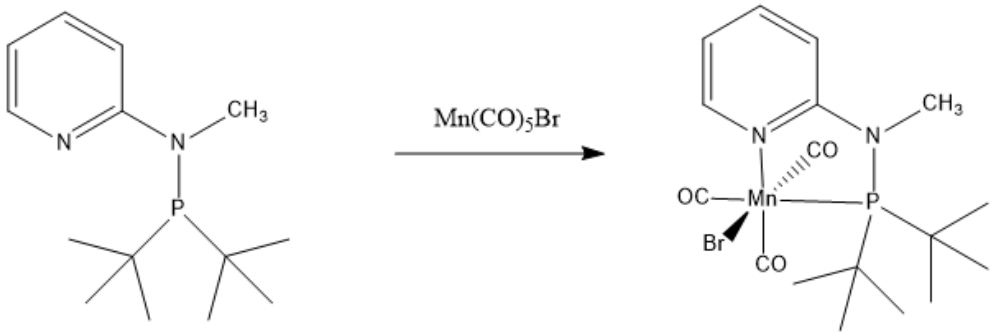

Scheme 2.13. Reaction scheme for the κ^2-([$(CH_3)_3C]_2$P)NMe(NC_5H_4)Mn$(CO)_3$Br compound.

In a glovebox, a solution of ([$(CH_3)_3C]_2$P)NH(NC_5H_4) ligand (0.126g, 0.5mmol) was prepared in 15mL of tetrahydrofuran. $Mn(CO)_5Br$ (0.137g, 0.5mmol) was added via stirring to the THF solution. The flask was wrapped in aluminum foil, removed from the glovebox and connected to a Schlenk line via a reflux condenser. The reaction was heated to 100^{o}C under N_2 and stirred for an additional 3 hours. The solution was cooled and the volume was reduced to ~3mL and 50mL of hexanes was added to get the complex as a sticky yellow-brown solid. The HNMR spectrum gave no desired signals. No crystals could be grown for single crystal analysis.

References

1. Rao, G. K.; Pell, W.; Korobkov, I.; Richeson, D. Electrocatalytic reduction of CO_2 using Mn complexes with unconventional coordination environments. *Chem. Commun*. **2016**, 52, 8010–8013.

2. Hameed, Y.; Gabidullin, B.; Richeson, D. Photocatalytic CO_2 Reduction with Manganese Complexes Bearing a κ^2-PN Ligand: Breaking the α-Diimine Hold on Group 7 Catalysts and Switching Selectivity. *Inorg. Chem*. **2018**, 57, 13092–13096.

3. Yang, Y.; Gurnham, J.; Liu, B.; Duchateau, R.; Gambarotta, S.; Korobkov, I. Selective ethylene oligomerization with chromium complexes bearing pyridine-phosphine ligands: influence of ligand structure on catalytic behavior. *Organometallics*. **2014**, 33, 5749–5757.

4. Macías-Arce, I.; Puerta, M. C.; Valerga, P. Half-Sandwich Benzylidene Ruthenium Complexes Bearing Phosphanyl-Pyridine Ligands: Reactivity towards Nucleophiles and Electrophiles. *Eur. J. Inorg. Chem*. **2010**, 2010, 1751–1751.

5. Blank, B.; Madalska, M.; Kempe, R. An Efficient Method for the Selective Iridium-Catalyzed Monoalkylation of (Hetero)aromatic Amines with Primary Alcohols. *Adv. Synth. Catal.* **2008**, 350, 749–758.

Chapter 3: Photocatalytic CO_2 Reduction with Manganese and Rhenium Complexes Bearing κ^2-PN Ligands

The work in this thesis aimed to synthesize various manganese and rhenium catalysts bearing phosphinoaminopyridine ligands and to test their photocatalytic ability to reduce CO_2. Second and third row transition metal complexes have been shown to function well as catalysts for the photochemical reduction of CO_2, and group 7 complexes have continued to hold a central position in CO_2 reduction since $MnX(bpy)(CO)_3$ was shown to be a good catalyst for photochemical reduction of CO_2 in 2014.[1,2] For this reason, rhenium was selected as a metal to synthesize catalysts, and manganese was selected because it is a more earth-abundant first row transition metal of group 7. The R group varies between either H or CH_3 in order to examine the effects of modifying the R group on the reactivity. For similar reasons, the R' groups phenyl, isopropyl, and tert-butyl were targeted. Furthermore, modification of the anionic groups was investigated. The starting materials with halo ligand X=Cl and X=Br were available and replacement of the halo ligand with triflate (OTf^-) was also investigated. The general structure for the catalysts investigated in this thesis is shown in Figure 3.1.

All of the complexes that were synthesized for this thesis were chosen in order to continue and expand upon previously published work from members of the Richeson lab.[1] In particular, initial investigations of the photocatalytic behaviour of two manganese and rhenium catalysts bearing PN ligands. κ^2-$(Ph_2P)NH(NC_5H_4)Re(CO)_3Br$ and κ^2-$(Ph_2P)NH(NC_5H_4)Mn(CO)_3Br$ (Figure 3.2) were both synthesised using the $(Ph_2P)NH(NC_5H_4)$ ligand, and showed *fac*-tricarbonyl coordination geometry. An analogous ligand, with N-Me rather than N-H, was used to prepare the related κ^2-$(Ph_2P)NMe(NC_5H_4)Mn(CO)_3Br$ compound (Figure 3.3), also showing *fac*-tricarbonyl coordination geometry. An additional manganese complex, κ^2-$(Ph_2P)NH(NC_5H_4)Mn(CO)_3OTf$ (Figure 3.4), was prepared with a ligand exchange reaction using AgOTf and κ^2-$(Ph_2P)NH(NC_5H_4)Mn(CO)_3Br$. The three manganese complexes all displayed similar Mn-N_{py} and Mn-P distances as well as N_{py}-Mn-P bite angles. The manganese catalysts all selectively produced CO as a

CO_2 reduction product. The catalyst bearing an N-H group yields higher TON than the analogous catalyst bearing an N-Me group. As well, when the bromide is switched to triflate, the TON decreased. The rhenium catalyst meanwhile selectively produced HCOOH as a CO_2 reduction product.

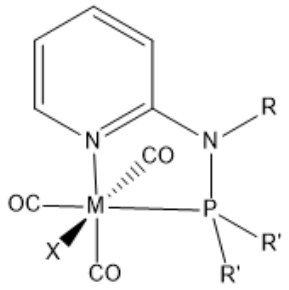

Figure 3.1. General structure of the catalysts investigated in this thesis.

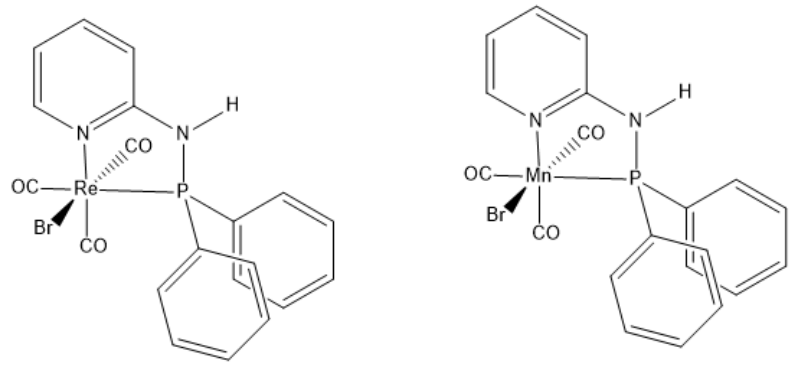

Figure 3.2. Structures of κ^2-$(Ph_2P)NH(NC_5H_4)Re(CO)_3Br$ and κ^2-$(Ph_2P)NH(NC_5H_4)Mn(CO)_3Br$.

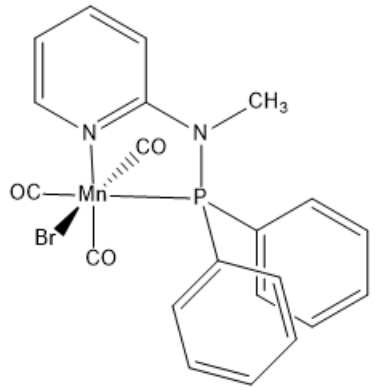

Figure 3.3. The structure of κ^2-$(Ph_2P)NMe(NC_5H_4)Mn(CO)_3Br$.

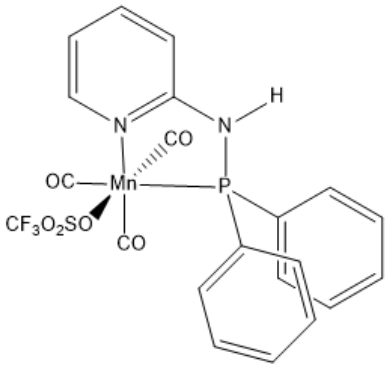

Figure 3.4. The structure of κ^2-$(Ph_2P)NH(NC_5H_4)Mn(CO)_3OTf$.

3.1 Photochemical Experiments: All of the photocatalytic reduction reactions with carbon dioxide were performed at room temperature in 20 mL sealed glass vials. Inside a glovebox, the photochemistry vials were prepared using the following procedure. In each vial, a measured amount of catalyst (solid) and photosensitizer (solid) were added with a small stir bar. To this mixture was added 1mL of the electron donor (ED) and 4mL of the solvent (S) via syringe. Finally, the vial is sealed using a crimper and an aluminum cap. Once the vials were prepared, the vials were purged with carbon dioxide for 20 minutes. The carbon dioxide is soluble in both DMF and DMA solvents, meaning that there is CO_2 both above and dissolved in the liquid phase. Once purged, the vials were placed in specific positions on a stir plate, and the photochemistry lights (blue lights centered at 450nm) were placed in fixed positions facing the vials. The reactions were stirred and irradiated for 24 hours.

3.1.1 Photochemistry Liquid Product Analysis

The liquid product formed from these photochemical reactions were analysed using NMR spectroscopy. In all cases the only product observed was formic acid, HCOOH. In order to quantify the amount of formic acid produced, the integral for the formyl proton was measured against an added quantity of dimethylsulfone, an internal standard. A standard solution containing 0.15g dimethyl sulfone (DMS) in 15mL of D_2O is prepared. DMS has a molar mass of 94.13g/mol and so the concentration of the standard solution can be found. 0.15g(1mol/94.13g)/0.015L= 0.1062mol/L. Using a syringe, 0.1mL of liquid from the reaction vial is placed into an NMR tube, along with 0.4mL of the DMS solution. 0.1062mol/L x 0.0004L = 0.00004249 mol DMS in the NMR tube. Since 0.1mL of the reaction solution is taken, this corresponds to a fraction of 0.1mL from 5mL total = 50. A ^{1}HNMR spectrum is obtained and analysed. The peak for DMS appears at ~3ppm as a singlet, which can be integrated. The peak for formic acid appears at ~8.3ppm as a singlet, which can also be integrated. In(DMS) and In(form) are the integrals for the two species. In(DMS) corresponds to 6 protons while In(form) corresponds to a single proton, and so

In(DMS) = 6 mol H/mol DMS x $4.249x10^{-5}$ mol DMS = 0.0002549 mol of H. If we take a ratio: In(form)/In(DMS) = XX mol H from formic/$2.549x10^{-4}$ mol H. Then XX mol H from formic = In(form)/In(DMS) x $2.549x10^{-4}$ mol H. Since formic acid corresponds to 1H this is also the mol of formic acid. We now need to multiply by 50 to get the total in the original sample: Amount of mol of formic acid = In(form)/In(DMS) x $2.549x10^{-4}$ x 50.

3.1.2 Photochemistry Gaseous Product Analysis

The gaseous products from these photochemical reactions, CO and H_2, were analysed with gas chromatography, using an Agilent 7820A GC equipped with a thermal conductivity detector (TCD) with an Agilent GS-CarbonPlot column (for CO_2) and Agilent HP-Molesieve column (for all other gasses). The oven was set to 45°C for 2.5 min, before the temperature was raised to 100°C at a rate of 20°C/minute. This was held for 12.75 minutes. Calibration curves with known quantities of CO and H_2 were prepared. After completion of the irradiation of the reaction mixture, a gas syringe was used to sample the headspace from the reaction vial and was injected into a gas chromatogram. The separation of analytes made their identification quite simple, H_2 elutes at 5.4 minutes, and CO eluted at 14 minutes. The area under the peaks of the chromatograms could be integrated and using the calibration curves the amounts of H_2 and CO could be calculated.

3.2 Electrochemical Experiments: Electrochemical experiments were carried out in a single compartment cell using a VersaSTAT 3 (Princeton Applied Research) potentiostat. A conventional three electrode system was employed consisting of a glassy carbon working electrode (diameter = 0.2 cm), a Pt wire as the auxiliary electrode, and an Ag wire as a pseudo-reference electrode. Ferrocene was added as a reference compound. Dried acetonitrile was purchased from Sigma Aldrich and stored on molecular sieves in glove-box. Tetrabutylammoniumhexafluorophosphate, $[(n\text{-}Bu)_4N]PF_6$ (TBAHFP), the supporting electrolyte, was crystallized two times with methanol, dried in vacuum at 90 °C for 24 h before use. The

electrolyte solution, 0.1 M $[(n\text{-}Bu)_4N]PF_6$ in CH_3CN, was saturated with N_2 by purging with N_2 for 10 min prior to each experiment. The typical concentration of catalyst was 1 mM (20 mL acetonitrile) in each experiment.

3.3 Previous Work

This thesis builds upon some initial work previously published by a PhD candidate, Yasmeen Hameed. The full details of which can be found in Reference 1.[1] Here I will present the relevant results of this work so that the results in this thesis may be compared to them.

Table 3.3 Photochemical results for 3 different catalysts using DMF as the solvent, TEOA as the electron donor, and $Ru(bpy)_3(PF_6)_2$ as the photosensitizer. Irradiation with blue light centered at 450nm for 24 hours. [1]

Catalyst	[catalyst] (mM)	[photosensitizer] (mM)	CO (μmol)	HCOOH (μmol)
κ^2-$(Ph_2P)NH(NC_5H_4)Mn(CO)_3Br$	0.2	0.2	14	-
	0.2	2	22	-
	0.1	0.1	4	-
	2	2	27	-
κ^2-$(Ph_2P)NMe(NC_5H_4)Mn(CO)_3Br$	0.2	0.2	5	-
	0.2	2	11	-
	0.1	0.1	3	-
	2	2	12	-
κ^2-$(Ph_2P)NH(NC_5H_4)Re(CO)_3Br$	0.2	0.2	-	59
	0.2	2	-	137
	0.1	0.1	-	48

3.4 Results

Photochemistry experiments were run using differing concentrations of catalyst and sensitizer. The amounts of HCOOH, H_2, and CO were determined using the techniques described above. Background experiments were also run, including background which contained all components except catalyst, and backgrounds which contained all components except CO_2. The background measurements of HCOOH were averaged and standard deviations were calculated. This average amount of HCOOH was subtracted from all HCOOH amounts obtained from the catalyst experiments. The HCOOH amounts presented in the tables have been corrected for background. More specifically, the HCOOH backgrounds and standard deviations for the experiments run in DMF were 44.7μmol (3.58) and for the experiments run in DMA were 40.9μmol (1.34). For CO the background measurements were quite variable. Because of this, any averaging would likely lead to errors in analysis. As a result, each individual background was subtracted from the corresponding amount. The CO amounts presented in the tables have been corrected for background. A similar variability in the amount of H_2 from the background measurements was observed. In some cases the background measurements actually exceeded the amount of H_2 produced during the full photocatalytic reaction. As a result, the H_2 amounts are presented in separate tables, with columns for the backgrounds included. For each catalyst, a table including the amount of product, turn over number (TON), turn over frequency (TOF), catalytic selectivity (CS), and quantum efficiency (ϕ) will be presented. All of these parameters were defined and explained in the introduction chapter.

Catalyst 1: κ^2-$(Ph_2P)NMe(NC_5H_4)Re(CO)_3Br$

Table 3.4.1. CO_2 reduction photochemistry results for the catalyst κ^2-$(Ph_2P)NMe(NC_5H_4)Re(CO)_3Br$. TEOA was used as the electron donor, and $Ru(bpy)_3(PF_6)_2$ as the photosensitizer. Irradiation with blue light centered at 450nm for 24 hours.

[Catalyst] (mM)	[Photosensitizer] (mM)	Solvent	HCOOH (μmol)	TON	TOF (hours^{-1})	CS	Φ (%)
2	2	DMF	77	8	0.3	15	3
1	1	DMF	46	9	0.4	18	2
0.2	2	DMF	187	187	8	21	6
0.1	1	DMF	74	148	6	11	3
0.2	0.2	DMF	37	37	2	10	1
0.1	0.1	DMF	27	54	2	10	1
2	2	DMA	109	11	0.5	4	4
1	1	DMA	181	36	2	100	6
0.2	2	DMA	137	137	6	11	5
0.1	1	DMA	52	105	4	4	2
0.2	0.2	DMA	47	47	2	6	2
0.1	0.1	DMA	12	25	1	3	0.4

Table 3.4.2. H_2 photochemistry results for the catalyst κ^2-$(Ph_2P)NMe(NC_5H_4)Re(CO)_3Br$. TEOA was used as the electron donor, and $Ru(bpy)_3(PF_6)_2$ as the photosensitizer. Irradiation with blue light centered at 450nm for 24 hours.

[Catalyst] (mM)	[Photosensitizer] (mM)	Solvent	H_2 (μmol)	H_2 Background under N_2	H_2 Background with no catalyst
2	2	DMF	5.3	2.1	6.3
1	1	DMF	2.5	0	3.2

0.2	2	DMF	8.7	2.2	6.3
0.1	1	DMF	6.8	0	3.2
0.2	0.2	DMF	3.6	0	2.3
0.1	0.1	DMF	2.8	0	0
2	2	DMA	27.4	26.6	6.1
1	1	DMA	0	9.3	3
0.2	2	DMA	12.6	31.1	6.1
0.1	1	DMA	14.9	10.2	3
0.2	0.2	DMA	8.2	5.3	2.3
0.1	0.1	DMA	4.4	0	0

Catalyst 1 selectively produced HCOOH as a CO_2 reduction product. This is consistent with prior results with similar catalysts[1], in which the manganese catalysts selectively gave CO as a product and the rhenium catalyst selectively gave HCOOH as a product. For catalyst 1 the best result for TON was 187, obtained in DMF solvent using 0.2mM catalyst and 2mM photosensitizer (Table 3.4.1, row 3). The same concentrations of catalyst and photosensitizer produced a TON of 137 using DMA solvent (Table 3.4.1, row 9). This catalyst produced good quantum efficiencies, comparable to those reported by Hameed.[1] Catalyst 1 also produced some H_2 gas as a product, however these results were varied and harder to interpret. The amount of H_2 produced during the photocatalytic experiment is in some cases lower than the amount of H_2 produced during the background experiments. This could indicate that the catalyst is not the only compound generating H_2, as it appears when no catalyst is present. $Ru(bpy)_3^{2+}$ may generate H_2, as the bpy ligand comes off and there is a vacant site to react.

Catalyst 2: κ^2-([$(CH_3)_2CH]_2$P)NMe(NC_5H_4)Re$(CO)_3$Br

Table 3.4.3. CO_2 reduction photochemistry results for the catalyst κ^2-([$(CH_3)_2CH]_2$P)NMe(NC_5H_4)Re$(CO)_3$Br. TEOA was used as the electron donor, and Ru$(bpy)_3(PF_6)_2$ as the photosensitizer. Irradiation with blue light centered at 450nm for 24 hours.

[Catalyst] (mM)	[Photosensitizer] (mM)	Solvent	HCOOH (μmol)	TON	TOF (hours^{-1})	CS	Φ (%)
2	2	DMF	86	9	0.4	5	3
1	1	DMF	115	23	1	14	4
0.2	2	DMF	55	55	2	3	2
0.1	1	DMF	5	9	0.4	1	0.2
0.2	0.2	DMF	0.2	0.2	0.009	100	0.007
0.1	0.1	DMF	10	20	0.8	100	0.3

Table 3.4.4. H_2 photochemistry results for the κ^2-([$(CH_3)_2CH]_2$P)NMe(NC_5H_4)Re$(CO)_3$Br catalyst. TEOA was used as the electron donor, and Ru$(bpy)_3(PF_6)_2$ as the photosensitizer. Irradiation with blue light centered at 450nm for 24 hours.

[Catalyst] (mM)	[Photosensitizer] (mM)	Solvent	H_2 (μmol)	H_2 background under N_2	H_2 background with no catalyst
2	2	DMF	16.5	6.3	6.3
1	1	DMF	7.9	0	3.2
0.2	2	DMF	17.5	11.2	6.3
0.1	1	DMF	4.4	5	3.2
0.2	0.2	DMF	0	0	2.3
0.1	0.1	DMF	0	0	0

Catalyst 2 selectively produced HCOOH as a CO_2 reduction product. Again, this is consistent with prior results[1], in which the manganese catalysts selectively gave CO as a product and the rhenium catalyst selectively gave HCOOH as a product. For catalyst 2 the best result for TON was 55, obtained in DMF solvent using 0.2mM catalyst and 2mM photosensitizer (Table 3.4.3, row 3). This catalyst produced good quantum efficiencies, comparable to those reported by Hameed.[1] Catalyst 2 also produced some H_2 gas as a product, however as with Catalyst 1, these results were varied and harder to interpret.

Catalyst 3: κ^2-([$(CH_3)_2CH]_2$P)NH(NC_5H_4)Re$(CO)_3$Br

Table 3.4.5. CO_2 reduction photochemistry results for the catalyst κ^2-([$(CH_3)_2CH]_2$P)NH(NC_5H_4)Re$(CO)_3$Br. TEOA was used as the electron donor, and Ru$(bpy)_3(PF_6)_2$ as the photosensitizer. Irradiation with blue light centered at 450nm for 24 hours.

[Catalyst] (mM)	[Photosensitizer] (mM)	Solvent	HCOOH (μmol)	TON	TOF (hours^{-1})	CS	Φ (%)
2	2	DMF	51	5	0.2	2	2
1	1	DMF	22	4	0.2	2	0.8
0.2	2	DMF	67	67	3	2	2
0.1	1	DMF	11	23	1	1	0.4
0.2	0.2	DMF	17	17	0.7	4	0.6
0.1	0.1	DMF	2	5	0.2	0.8	0.08
2	2	DMA	31	3	0.1	1	1
1	1	DMA	15	3	0.1	1	0.5
0.2	2	DMA	35	35	1	2	1
0.1	1	DMA	7	14	0.6	1	0.2
0.2	0.2	DMA	3	3	0.1	0.8	0.09
0.1	0.1	DMA	3	5	0.2	100	0.09

Table 3.4.6. H_2 photochemistry results for the κ^2-([$(CH_3)_2CH]_2$P)NH(NC_5H_4)Re$(CO)_3$Br catalyst. TEOA was used as the electron donor, and Ru$(bpy)_3(PF_6)_2$ as the photosensitizer. Irradiation with blue light centered at 450nm for 24 hours.

[Catalyst] (mM)	[Photosensitizer] (mM)	Solvent	H_2 (μmol)	H_2 background under N_2	H_2 background with no catalyst
2	2	DMF	22.8	28.6	6.3
1	1	DMF	13.4	9.3	3.2
0.2	2	DMF	26.9	9.3	6.3
0.1	1	DMF	8.2	0	3.2
0.2	0.2	DMF	4.3	0	2.3
0.1	0.1	DMF	3	0	0
2	2	DMA	23.9	32.8	6.1
1	1	DMA	12.7	16.5	3
0.2	2	DMA	20.9	27	6.1
0.1	1	DMA	4.8	13	3
0.2	0.2	DMA	3.4	2.9	2.3
0.1	0.1	DMA	0	0	0

Catalyst 3 selectively produced HCOOH as a CO_2 reduction product as would be expected based on previous results[1], in which the manganese catalysts selectively gave CO as a product and the rhenium catalyst selectively gave HCOOH as a product. For catalyst 3 the best result for TON was 67, obtained in DMF solvent using 0.2mM catalyst and 2mM photosensitizer (Table 3.4.5, row 3). The same concentrations of catalyst and photosensitizer produced a TON of 35 using DMA solvent (Table 3.4.5, row 9). This catalyst produced good quantum efficiencies, comparable to those reported by Hameed.[1]

Catalyst 3 also produced some H_2 gas as a product, however similar to Catalysts 1&2, these results were varied and harder to interpret.

Catalyst 4: $[\kappa^2\text{-}[([(CH_3)_2CH]_2PO)NH(NC_5H_4)]_2MnBr]^{1+}\ Br^-$

Table 3.4.7. CO_2 reduction photochemistry results for the catalyst $[\kappa^2\text{-}[([(CH_3)_2CH]_2PO)NH(NC_5H_4)]_2MnBr]^{1+}\ Br^-$. TEOA was used as the electron donor, and $Ru(bpy)_3(PF_6)_2$ as the photosensitizer. Irradiation with blue light centered at 450nm for 24 hours.

[Catalyst] (mM)	[Photosensitizer] (mM)	Solvent	CO (μmol)	TON	TOF (hours^{-1})	CS	Φ (%)
2	2	DMF	26	3	0.1	6	0.9
1	1	DMF	11	2	0.09	3	0.4
0.2	2	DMF	11	11	0.5	1	0.4
0.1	1	DMF	11	22	0.9	2	0.4
0.2	0.2	DMF	8	8	0.3	100	0.3
0.1	0.1	DMF	5	11	0.5	100	0.2
2	2	DMA	17	2	0.07	3	0.6
1	1	DMA	3	0.7	0.03	100	0.1
0.2	2	DMA	12	12	0.5	0.7	0.4
0.1	1	DMA	17	34	1	7	0.6
0.2	0.2	DMA	8	8	0.3	100	0.3
0.1	0.1	DMA	0	0	0	0	0

Table 3.4.8. H_2 photochemistry results for the $[\kappa^2\text{-}[([(CH_3)_2CH]_2PO)NH(NC_5H_4)]_2MnBr]^{1+}$ Br^- catalyst. TEOA was used as the electron donor, and $Ru(bpy)_3(PF_6)_2$ as the photosensitizer. Irradiation with blue light centered at 450nm for 24 hours.

[Catalyst] (mM)	[Photosensitizer] (mM)	Solvent	H_2 (μmol)	H_2 background under N_2	H_2 background with no catalyst
2	2	DMF	4.6	5.1	6.3
1	1	DMF	3.3	0	3.2
0.2	2	DMF	10.5	5	6.3
0.1	1	DMF	5.8	0	3.2
0.2	0.2	DMF	0	0	2.3
0.1	0.1	DMF	0	0	0
2	2	DMA	6.4	11	6.1
1	1	DMA	0	3.9	3
0.2	2	DMA	17	6.9	6.1
0.1	1	DMA	2.6	2.4	3
0.2	0.2	DMA	0	2	2.3
0.1	0.1	DMA	0	0	0

Catalyst 4 selectively produced CO as a CO_2 reduction product. For catalyst 4 the best result for TON was 34, obtained in DMA solvent using 0.1mM catalyst and 1mM photosensitizer (Table 3.4.7, row 10). The same concentrations of catalyst and photosensitizer produced a TON of 22 in DMF solvent (Table 3.4.7, row 4). This catalyst is completely different in both coordination geometry and oxidation state when compared to catalysts 1, 2, and 3. Additionally, the phosphinoaminopyridine ligand is oxidized, which is a change from the reported ligands currently used for CO_2 reduction. The Mn(II) metal center, combined with this oxidized phosphinoaminopyridine ligand create a novel catalyst for CO_2 reduction. The selectivity of this novel catalyst for CO production is therefore a new feature. It is interesting that

although it is different in oxidation state and coordination geometry from the previous Mn catalysts containing phosphinoaminopyridine ligands, that it exhibits a similar selectivity for CO. This catalyst produced good quantum efficiencies, however they are lower than the quantum efficiencies for the previous 3 rhenium catalysts. Catalyst 4 also produced some H_2 gas as a product, however again these results were varied and harder to interpret.

The catalysts presented in this thesis all contain various phosphinoaminopyridine ligands and group 7 metal centers. Group 7 complexes that have been reported as CO_2 photoreduction catalysts have largely been limited to bidentate α-dimmine ligands. The phosphinoaminopyridine ligands used in this thesis replace a pyridine moiety with a more basic phosphine donor, and lack the π conjugation of the bpy scaffold. $Re^{I}(bpy)(CO)_3X$ complexes were first investigated in the 1980's as photocatalysts for CO_2 reduction.

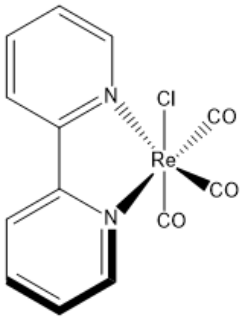

Figure 3.4.1 The structure of $[Re^{I}(bpy)(CO)_3Cl]$ complex.

These $Re^{I}(bpy)(CO)_3X$ complexes show high quantum efficiencies for their ability to reduce CO_2 selectively to CO.[3,4,5] The manganese analogues were investigated in 2014 as catalysts for the photochemical reduction of CO_2. In photocatalytic CO_2 reductions, *fac*-$[Mn^{I}(bpy)(CO)_3Br]$ was reported as an efficient type I catalyst for CO_2 reduction. It has been shown to selectively produce formate.[6,7]

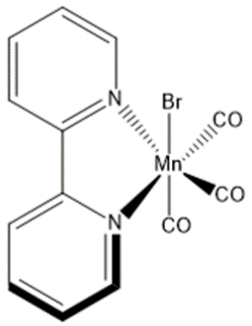

Figure 3.4.2 The structure of [Mn^{I}(bpy)$(CO)_3$Br] complex.

The Re catalysts presented in this thesis (Catalysts 1, 2, and 3) show opposite selectivity to these Re^{I}(bpy)$(CO)_3$X complexes. All three of the Re catalysts presented in this thesis display the same selectivity for HCOOH as the analogous κ^2-$(Ph_2P)NH(NC_5H_4)Re(CO)_3Br$ catalyst reported by Hameed.[1] These results contribute three new Re catalysts with excellent selectivity to the field of photocatalytic CO_2 reduction. The novel Mn(II) catalyst (Catalyst 4), displays a different oxidation number and coordination geometry to the previously reported Mn catalysts, as well as having oxidized phosphinoaminopyridine ligands. This catalyst is not an analogue of the reported Mn catalysts[1] and so unfortunately, it cannot be directly compared to them. However, this catalyst does show an excellent selectivity for CO, and this result is promising in showing that moving away from the dimmine ligand framework produces highly selective photoreduction catalysts.

The differing selectivity for either CO or HCOOH displayed by photoreduction catalysts can be explained using Scheme 3.4.1. There are several different pathways through which CO_2 reduction may proceed, giving an array of reduction products. Metal hydride intermediate formation is believed to influence the products of CO_2 reduction. Reaction of CO_2 with molecular complexes usually occurs either by insertion into a metal-hydride bond, or by binding to a vacant coordination site at the metal center (Scheme 3.4.1).[8]

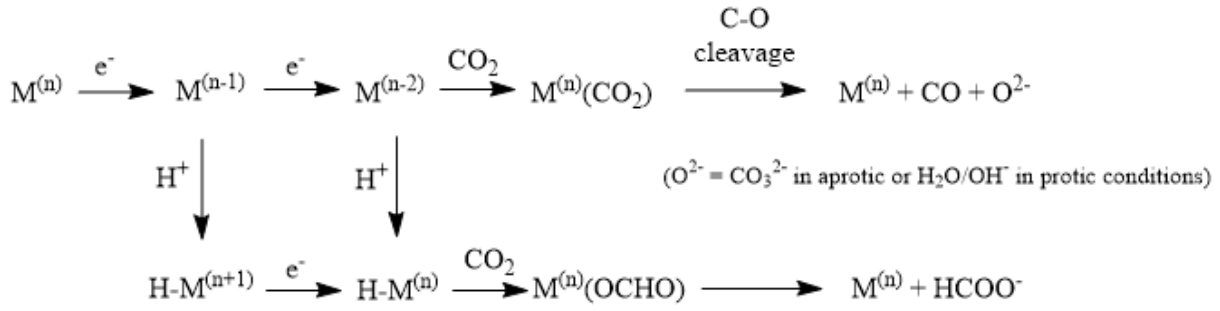

Scheme 3.4.1. Competing pathways for HCOOH and CO formation from CO_2 reduction.[8]

The usual pathway by which CO_2 inserts into a metal-hydride is thought to be promoted by electrostatic interactions between the polarized O-C and M-H bonds, positioning the electrophilic carbon atom in close proximity to the nucleophilic hydride moiety. Electron rich metals possessing free binding sites favour CO_2 activation through monodentate C-coordination. This leads to a metallo-carboxylate species with O-atoms sterically exposed and available for protonation. Both insertion and coordination may proceed through different routes that vary in the mode of CO_2 interaction with the metal center, however insertion typically favours HCOOH as a product and coordination typically favours CO as a product.[8]

Turn over number (TON) is another parameter by which to compare various catalysts. The highest TON for all three rhenium catalysts occurred using the same conditions: 0.2mM catalyst, 2mM photosensitizer, and DMF solvent. The same concentration conditions produced the highest TON in the DMA solvent as well. Again, this is consistent with previous results that were observed for a single Re analogue, in which the highest TON occurred for the conditions of 0.2mM catalyst and 2mM photosensitizer. The highest TON displayed for the novel Mn catalyst (4) was 34, which occurred in DMA solvent using 0.1mM catalyst and 1mM photosensitizer. The same concentrations of catalyst and photosensitizer produced a TON of 22 in DMF solvent. As previously mentioned, this catalyst 4 is not an

analogue of the reported Mn catalysts[1], however TONs of 34 and 22 are comparable to those reported. This result is exciting, as a novel catalyst is shown to have TONs comparable to those already reported in literature.

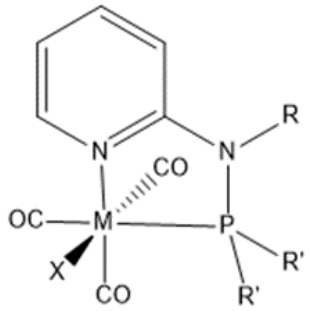

Figure 3.4.3. General structure of catalysts investigated in this thesis.

When comparing the different substituents present on the catalysts, another pattern involving the TON can be determined. Changing the R substituent between H and CH_3 affects the reactivity of the catalysts, with R=H producing a higher TON than R=CH_3. Catalyst 2 (κ^2-([$(CH_3)_2CH]_2$P)NMe(NC_5H_4)Re$(CO)_3$Br) and catalyst 3 (κ^2-([$(CH_3)_2CH]_2$P)NH(NC_5H_4)Re$(CO)_3$Br) are analogous to one another, with the only difference being either an H or CH_3 group present on the nitrogen. Catalyst 2 produces a TON of 55, while catalyst 3 produces a TON of 67. Catalyst 1 (κ^2-(Ph_2P)NMe(NC_5H_4)Re$(CO)_3$Br) is analogous to the reported Re catalyst (κ^2-(Ph_2P)NH(NC_5H_4)Re$(CO)_3$Br)[1], again the only difference being the substituent on the nitrogen. Catalyst 1 bearing a methyl group produced a TON of 187, whereas the reported Re catalyst bearing a hydrogen produced a TON of 343. Both of these pairs of analogous compounds display higher TON when R=H. A possible explanation for this behaviour is the electron donating ability of the R groups. The methyl R group is more electron donating than the hydrogen R group, which puts more electron density on the ligand and metal. This added electron density could make the catalyst more difficult to reduce, leading to a lower TON when using the methyl R substituent.

This thesis also explored the effect of changing the R' substituents on the reactivity of the various catalysts. The reported Re catalyst[1] only contains R'=phenyl, and in this work R'=phenyl and R'=isopropyl were both successfully used in Re catalysts. Changing this R' substituent does in fact have an effect on the reactivity of the Re catalysts, with R'=phenyl producing higher TON than R'=isopropyl. Catalyst 1 (κ^2-$(Ph_2P)NMe(NC_5H_4)Re(CO)_3Br$) and Catalyst 2 ($\kappa^2$-$([(CH_3)_2CH]_2P)NMe(NC_5H_4)Re(CO)_3Br$) are analogous to one another, with the only difference being the R' substituents of either phenyl (1) or isopropyl (2). Catalyst 1 produced a TON 187, whereas the analogous catalyst 2 produced a TON of 55. Catalyst 3 (κ^2-$([(CH_3)_2CH]_2P)NH(NC_5H_4)Re(CO)_3Br$) is analogous to the reported Re catalyst (κ^2-$(Ph_2P)NH(NC_5H_4)Re(CO)_3Br$)[1], again the only difference being the R' substituents. Catalyst 3 bearing two isopropyl substituents produced a TON of 67, whereas the reported Re catalyst bearing two phenyl substituents produced a TON of 343. Both of these analogous pairs display higher TON when R'=phenyl. Following the logic presented for the R substituents, a possible explanation for this behaviour is the electron donating ability of the R' groups. The isopropyl R group is more electron donating than the phenyl R group, which puts more electron density on the ligand and metal. This added electron density could make the catalyst more difficult to reduce, leading to a lower TON when using the isopropyl R substituent.

Comparing the three rhenium catalysts presented in this work with the reported Re catalyst[1], the highest TON was achieved by the reported Re catalyst, with a TON of 343, followed by Catalyst 1 with a TON of 187, Catalyst 3 with a TON of 67, and finally Catalyst 2 with a TON of 55. While these three new Re catalysts have TONs lower than the reported compound, they all still show excellent selectivity and good TONs. These results are important because they also exhibit the effect that changing the ligand substituents has on the reactivity of the catalyst. When comparing all four of these catalysts, the best catalyst contains R=H and R'=phenyl, second best contains R=CH_3 and R'=phenyl, third best contains R=H and R'=isopropyl, and fourth best contains R=CH_3 and R'=isopropyl. Above, it was shown that R=H

produces higher TON than R=CH_3 and that R'=phenyl produces higher TON than R'=isopropyl. Comparing all four analogous compounds, it is evident that the R' substituent has a greater effect on the TON. Having R'=phenyl with R=CH_3 in catalyst 1 produces a higher TON than catalyst 3 containing R'=isopropyl and R=H.

These results are exciting as four new catalysts for the photocatalytic reduction of CO_2 were presented. Three new Re photoreduction catalysts were successfully synthesized and displayed good TON and excellent selectivity for HCOOH formation. These catalysts are similar in both structure and reactivity to the Re catalyst previously reported for catalytic CO_2 reduction.[1] Additionally, a novel Mn(II) catalyst with oxidized phosphinoaminopyridine ligands was successfully synthesised and displayed good TON and excellent selectivity for CO formation. In this work, it was shown that changing the R and R' substituents present on the phosphinoaminopyridine ligands influences the catalyst's reactivity.

References

1. Hameed, Y.; Gabidullin, B.; Richeson, D. Photocatalytic CO_2 Reduction with Manganese Complexes Bearing a κ2-PN Ligand: Breaking the α-Diimine Hold on Group 7 Catalysts and Switching Selectivity. *Inorganic Chemistry* **2018**, *57* (21), 13092.

2. H. Takeda, H. Koizumi, K. Okamoto and O. Ishitani. Photocatalytic CO_2 reduction using a Mn complex as a catalyst. *Chem. Commun*., **2014**, 50, 1491–1493.

3. A. J. Morris, G. J. Meyer and E. Fujita. Molecular approaches to the photocatalytic reduction of carbon dioxide for solar fuels. *Acc. Chem. Res*., **2009**, 42, 1983–1994.

4. J. Hawecker, J.-M. Lehn and R. Ziessel. Efficient Photochemical Reduction of CO_2 to CO by Visible Light Irradiation of Systems containing $Re(bipy)(CO)_3X$ or $Ru(bipy)_3^{2+}$-Co^{2+} Combinations as Homogeneous Catalysts. *J. Chem. Soc. Chem. Commun*., **1983**, 536–538.

5. J. Hawecker, J. Lehn and R. Ziessel. Photochemical and Electrochemical Reduction of Carbon Dioxide to Carbon Monoxide Mediated by (2,2'-Bipyridine)tricarbonylchlororhenium(I) and Related Complexes as Homogeneous Catalysts). *Helv. Chim. Acta*, **1986**, 69, 1990–2012.

6. Y. Yamazaki, H. Takeda and O. Ishitani. Photocatalytic reduction of CO2 using metal complexes. *J. Photochem. Photobiol. C Photochem. Rev*., **2015**, 25, 106–137.

7. H. Takeda, H. Koizumi, K. Okamoto and O. Ishitani. Photocatalytic CO_2 reduction using a Mn complex as a catalyst. *Chem. Commun*., **2014**, 50, 1491–1493.

8. Dalle, K. E.; Warnan, J.; Leung, J. J.; Reuillard, B.; Karmel, I. S.; Reisner, E. Electro- and Solar-Driven Fuel Synthesis with First Row Transition Metal Complexes. *Chem. Rev*. **2019**, 119, 2752–2875.

Chapter 4: Conclusions and Future Directions

4.1 Conclusion

This thesis investigated photocatalytic CO_2 reduction using manganese and rhenium catalysts containing bidentate phosphinoaminopyridine ligands. In chapter 1 the background surrounding photocatalytic CO_2 reduction was presented, along with examples of catalysts that have been previously shown to reduce CO_2. In chapter 2, the synthesis and characterization were presented for several ligands along with a variety of transition metal complexes. The ligands varied in their substituents, so that the effect of this change could be noted on the catalyst performance. Four of the transition metal complexes that were successfully prepared are in fact novel structures. In chapter 3, these four new catalysts were successfully tested under different photocatalytic conditions. All catalysts displayed good TON and excellent selectivity. All three of the Re catalysts presented in this thesis display excellent selectivity for HCOOH. The novel Mn(II) catalyst displays a different oxidation number and coordination geometry to the previously reported Mn catalysts, as well as having oxidized phosphinoaminopyridine ligands. This catalyst displays an excellent selectivity for CO, as well as good TON. Changing the R and R' substituents on the phosphinoaminopyridine ligands was also shown to have an effect on the catalyst activity. These results are promising in showing that moving away from the dimmine ligand framework produces highly selective photoreduction catalysts which display good TONs.

4.2 Future Directions

While this thesis has presented four novel catalysts for photocatalytic CO_2 reduction, further work could still be done with this project. Further investigation of the electrochemical behaviour of the four catalysts is needed in order to completely characterize these novel compounds. As well, computations should be done on the structures of these compounds, possibly using density functional theory (DFT)

computational methods. As well, several of the complexes that were presented in chapter 2 were not synthesized successfully, and so future work on this project may include re-synthesising these compounds using alternative methods in order to attain the correct product. Continued modification of the phosphinoaminopyridine ligand to include other substituents on both the nitrogen and phosphorus would also further the understanding of the role these play in the catalytic behaviour. The catalysts presented in this thesis should also be tested under different photochemical conditions, such as with new electron donors and different photosensitizers. Finally, while rhenium and manganese are good choices for metal centers, a shift to more abundant first row transition metals should also be a focus for anyone pursuing this project in the future.

Appendix A: Complete Crystallographic Data Set for κ^2-$(Ph_2P)NMe(NC_5H_4)Re(CO)_3Br$

Bond Lengths κ^2-$(Ph_2P)NMe(NC_5H_4)Re(CO)_3Br$						
Atom	**Atom**	**Length (Å)**		**Atom**	**Atom**	**Length (Å)**
Re1	C1	1.880(8)		C4	C5	1.365(12)
Re1	C2	1.932(9)		C5	C6	1.384(14)
Re1	C3	1.959(10)		C6	C7	1.352(14)
Re1	N1	2.199(5)		C7	C8	1.416(11)
Re1	P1	2.404(2)		C10	C15	1.365(12)
Re1	Br1	2.6143(9)		C10	C11	1.400(12)
P1	N2	1.702(6)		C11	C12	1.368(13)
P1	C16	1.813(8)		C12	C13	1.380(17)
P1	C10	1.817(8)		C13	C14	1.380(17)
O1	C1	1.195(10)		C14	C15	1.399(12)
O2	C2	1.185(11)		C16	C21	1.380(11)
O3	C3	1.056(11)		C16	C17	1.407(11)
N1	C8	1.348(12)		C17	C18	1.384(12)
N1	C4	1.349(12)		C18	C19	1.381(13)
N2	C8	1.377(10)		C19	C20	1.398(12)
N2	C9	1.486(11)		C20	C21	1.386(14)

Bond Angles κ^2-$(Ph_2P)NMe(NC_5H_4)Re(CO)_3Br$								
Atom	**Atom**	**Atom**	**Angle (˚)**		**Atom**	**Atom**	**Atom**	**Angle (˚)**
C1	Re1	C2	89.2(4)		O1	C1	Re1	175.4(9)
C1	Re1	C3	90.8(3)		O2	C2	Re1	177.8(8)
C2	Re1	C3	90.3(4)		O3	C3	Re1	177.1(7)
C1	Re1	N1	173.1(5)		N1	C4	C5	123.8(8)
C2	Re1	N1	97.1(3)		C4	C5	C6	118.4(8)
C3	Re1	N1	92.0(3)		C7	C6	C5	119.3(7)
C1	Re1	P1	95.9(3)		C6	C7	C8	120.4(8)
C2	Re1	P1	171.9(2)		N1	C8	N2	118.9(7)
C3	Re1	P1	95.9(3)		N1	C8	C7	120.0(7)
N1	Re1	P1	77.5(3)		N2	C8	C7	121.1(7)
C1	Re1	Br1	94.4(3)		C15	C10	C11	119.1(8)
C2	Re1	Br1	87.1(3)		C15	C10	P1	125.2(7)
C3	Re1	Br1	174.2(2)		C11	C10	P1	115.8(6)
N1	Re1	Br1	83.2(2)		C12	C11	C10	120.3(9)
P1	Re1	Br1	86.29(6)		C11	C12	C13	121.1(10)
N2	P1	C16	106.3(3)		C14	C13	C12	118.9(9)
N2	P1	C10	102.9(3)		C13	C14	C15	120.3(10)
C16	P1	C10	106.1(4)		C10	C15	C14	120.4(10)
N2	P1	Re1	102.2(2)		C21	C16	C17	118.7(8)
C16	P1	Re1	116.8(3)		C21	C16	P1	123.1(6)
C10	P1	Re1	120.7(3)		C17	C16	P1	118.2(6)
C8	N1	C4	118.2(6)		C18	C17	C16	120.2(8)
C8	N1	Re1	121.2(6)		C19	C18	C17	120.9(8)

C4	N1	Re1	120.6(6)		C18	C19	C20	118.9(10)
C8	N2	C9	118.9(6)		C21	C20	C19	120.4(9)
C8	N2	P1	119.6(5)		C16	C21	C20	120.8(7)
C9	N2	P1	120.1(5)					

Hydrogen Bonds for κ^2-(Ph_2P)NMe(NC_5H_4)Re($CO)_3$Br						
D	**H**	**A**	**d(D-H) (Å)**	**d(H-A) (Å)**	**d(D-A) (Å)**	**D-H-A (°)**
C4	H4	$Br1^1$	0.94	2.84	3.545(9)	133.0
C5	H5	$Br1^1$	0.94	3.03	3.624(9)	122.3
C7	H7	$Br1^2$	0.94	3.11	3.693(8)	121.5

Hydrogen Atom Coordinates (Å×10^4) and Isotropic Displacement Parameters (Å^2×10^3) for κ^2-(Ph_2P)NMe(NC_5H_4)Re($CO)_3$Br				
Atom	***x***	***y***	***z***	**U(eq)**
H4	8337.41	7911.46	9298.72	37
H5	6370.67	7968.89	10268.56	44
H6	4502.83	6378.72	10051.58	43
H7	4623.17	4837.99	8821.06	37
H9A	5350.53	3205.36	7958.47	53
H9B	5468.82	3136.73	6652.8	53
H9C	4232.35	4055.72	6952.24	53
H11	5327.12	5999.82	5511.33	46
H12	3482.24	6070.01	3602.19	66
H13	3731.82	4754.57	2164.23	68
H14	5829.38	3317.58	2687.42	62
H15	7686.02	3224.51	4630.56	53
H17	10525.93	3611.49	5903.99	38
H18	12028.16	1855.31	6174.54	47
H19	11694.1	434.14	7497.23	50
H20	9891.16	824.93	8611.71	44
H21	8332.58	2559.44	8310.37	34

Appendix B: Complete Crystallographic Data Set for κ^2-([(CH$_3$)$_2$CH]$_2$P)NMe(NC$_5$H$_4$)Re(CO)$_3$Br

Bond Lengths for κ^2-([(CH$_3$)$_2$CH]$_2$P)NMe(NC$_5$H$_4$)Re(CO)$_3$Br						
Atom	**Atom**	**Length (Å)**		**Atom**	**Atom**	**Length (Å)**
Re1	C1	1.919(3)		N1	C11	1.379(4)
Re1	C3	1.923(4)		N1	C10	1.478(4)
Re1	C2	1.971(4)		N2	C11	1.360(4)
Re1	N2	2.202(3)		N2	C15	1.361(4)
Re1	P1	2.4237(15)		C4	C6	1.520(5)
Re1	Br1	2.6427(13)		C4	C5	1.533(5)
P1	N1	1.712(3)		C7	C9	1.521(5)
P1	C7	1.850(4)		C7	C8	1.527(5)
P1	C4	1.862(3)		C11	C12	1.411(4)
O1	C1	1.153(4)		C12	C13	1.359(5)
O2	C2	1.132(4)		C13	C14	1.383(6)
O3	C3	1.093(4)		C14	C15	1.353(5)

Bond Angles for κ^2-([(CH$_3$)$_2$CH]$_2$P)NMe(NC$_5$H$_4$)Re(CO)$_3$Br								
Atom	**Atom**	**Atom**	**Angle (˚)**		**Atom**	**Atom**	**Atom**	**Angle (˚)**
C1	Re1	C3	88.33(14)		C11	N1	P1	120.4(2)
C1	Re1	C2	92.18(13)		C10	N1	P1	120.4(2)
C3	Re1	C2	87.82(13)		C11	N2	C15	117.3(3)
C1	Re1	N2	171.91(11)		C11	N2	Re1	121.6(2)
C3	Re1	N2	95.15(12)		C15	N2	Re1	121.0(2)
C2	Re1	N2	95.25(12)		O1	C1	Re1	176.3(3)
C1	Re1	P1	94.87(10)		O2	C2	Re1	178.8(3)
C3	Re1	P1	93.91(9)		O3	C3	Re1	174.4(3)
C2	Re1	P1	172.79(10)		C6	C4	C5	109.6(3)
N2	Re1	P1	77.63(8)		C6	C4	P1	113.3(3)
C1	Re1	Br1	90.62(10)		C5	C4	P1	109.8(2)
C3	Re1	Br1	171.98(9)		C9	C7	C8	110.7(3)
C2	Re1	Br1	84.27(9)		C9	C7	P1	112.8(3)
N2	Re1	Br1	86.93(7)		C8	C7	P1	110.9(3)
P1	Re1	Br1	94.11(2)		N2	C11	N1	118.4(3)
N1	P1	C7	103.64(16)		N2	C11	C12	120.3(3)
N1	P1	C4	105.68(15)		N1	C11	C12	121.4(3)
C7	P1	C4	102.83(17)		C13	C12	C11	120.1(4)
N1	P1	Re1	101.81(11)		C12	C13	C14	119.5(3)
C7	P1	Re1	117.88(12)		C15	C14	C13	118.5(4)
C4	P1	Re1	122.86(12)		C14	C15	N2	124.2(4)
C11	N1	C10	119.2(3)					

Hydrogen Bonds for κ^2-([(CH$_3$)$_2$CH]$_2$P)NMe(NC$_5$H$_4$)Re(CO)$_3$Br						
D	**H**	**A**	**d(D-H) (Å)**	**d(H-A) (Å)**	**d(D-A) (Å)**	**D-H-A (°)**
C5	H5C	Br1	0.97	3.03	3.837(4)	142.0

C6	H6B	Br1	0.97	2.83	3.700(4)	149.2
C7	H7	O3[1]	0.99	2.62	3.575(5)	161.1
C8	H8A	O2[1]	0.97	2.55	3.472(5)	159.4
C9	H9C	O3	0.97	2.47	3.409(5)	163.0

Torsion Angles for κ^2-([$(CH_3)_2CH]_2$P)NMe(NC_5H_4)Re($CO)_3$Br										
A	**B**	**C**	**D**	**Angle (˚)**		**A**	**B**	**C**	**D**	**Angle (˚)**
C7	P1	N1	C11	124.0(3)		Re1	P1	C7	C8	-57.9(3)
C4	P1	N1	C11	-128.3(3)		C15	N2	C11	N1	176.7(3)
Re1	P1	N1	C11	1.1(3)		Re1	N2	C11	N1	-5.3(4)
C7	P1	N1	C10	-55.2(3)		C15	N2	C11	C12	-3.9(4)
C4	P1	N1	C10	52.6(3)		Re1	N2	C11	C12	174.1(2)
Re1	P1	N1	C10	-178.1(2)		C10	N1	C11	N2	-178.5(3)
N1	P1	C4	C6	38.1(3)		P1	N1	C11	N2	2.3(4)
C7	P1	C4	C6	146.5(3)		C10	N1	C11	C12	2.1(5)
Re1	P1	C4	C6	-77.6(3)		P1	N1	C11	C12	-177.1(2)
N1	P1	C4	C5	161.1(3)		N2	C11	C12	C13	2.8(5)
C7	P1	C4	C5	-90.6(3)		N1	C11	C12	C13	-177.8(3)
Re1	P1	C4	C5	45.3(3)		C11	C12	C13	C14	0.1(5)
N1	P1	C7	C9	-44.6(3)		C12	C13	C14	C15	-1.6(5)
C4	P1	C7	C9	-154.5(3)		C13	C14	C15	N2	0.4(5)
Re1	P1	C7	C9	66.9(3)		C11	N2	C15	C14	2.4(5)
N1	P1	C7	C8	-169.4(3)		Re1	N2	C15	C14	-175.7(3)
C4	P1	C7	C8	80.6(3)						

Hydrogen Atom Coordinates (Å×10^4) and Isotropic Displacement Parameters (Å^2×10^3) for κ^2-([$(CH_3)_2CH]_2$P)NMe(NC_5H_4)Re($CO)_3$Br				
Atom	***x***	***y***	***z***	**U(eq)**
H4	7239.16	3321.58	8787.04	37
H5A	7978.2	4138.4	10361.96	66
H5B	6894.19	4790.55	9811.39	66
H5C	8241.08	5124.4	9719.94	66
H6A	9369.2	3337.47	9210.44	63
H6B	9442.98	4232.11	8384.43	63
H6C	8979.89	3166.27	7961.56	63
H7	5359.31	3533.07	7709.83	40
H8A	3871.05	4632.66	8279.03	98
H8B	4788.87	5532.69	8233.52	98
H8C	5085.15	4647.85	9068.36	98
H9A	3840.09	4102.51	6417.07	62
H9B	5050.35	3952.92	5880.49	62
H9C	4632.02	5043.44	6174.49	62
H10A	6779.66	2900.25	5566.86	65
H10B	6942.58	2724.74	6833.06	65
H10C	8085.23	2743.87	6182.91	65

H12	8093.57	3599.3	4539.07	47
H13	8935.76	4595.73	3312.8	55
H14	9245.08	6297.85	3687.64	50
H15	8636.44	6946.51	5227.21	38

Appendix C: Complete Crystallographic Data Set for κ^2-([$(CH_3)_2CH]_2$P)NH(NC_5H_4)Re$(CO)_3$Br

Bond Lengths for κ^2-([$(CH_3)_2CH]_2$P)NH(NC_5H_4)Re$(CO)_3$Br						
Atom	**Atom**	**Length (Å)**		**Atom**	**Atom**	**Length (Å)**
Re1	C2	1.921(10)		O3	C3	1.145(11)
Re1	C3	1.928(9)		C2	O2	1.118(11)
Re1	C1	1.962(10)		N2	C8	1.386(10)
Re1	N1	2.210(6)		C4	C5	1.369(13)
Re1	P1	2.430(2)		C8	C7	1.402(11)
Re1	Br1	2.5833(12)		C7	C6	1.380(13)
P1	N2	1.692(7)		C6	C5	1.397(14)
P1	C9	1.834(9)		C9	C11	1.524(14)
P1	C12	1.855(11)		C9	C10	1.532(14)
N1	C4	1.351(10)		C12	C13	1.521(17)
N1	C8	1.352(11)		C12	C14	1.529(15)
O1	C1	1.137(11)				

Bond Angles for κ^2-([$(CH_3)_2CH]_2$P)NH(NC_5H_4)Re$(CO)_3$Br								
Atom	**Atom**	**Atom**	**Angle (˚)**		**Atom**	**Atom**	**Atom**	**Angle (˚)**
C2	Re1	C3	88.0(4)		C4	N1	C8	117.7(7)
C2	Re1	C1	90.7(4)		C4	N1	Re1	122.3(6)
C3	Re1	C1	90.1(4)		C8	N1	Re1	119.6(5)
C2	Re1	N1	96.2(3)		O1	C1	Re1	179.4(9)
C3	Re1	N1	174.1(3)		O3	C3	Re1	178.4(8)
C1	Re1	N1	94.1(3)		O2	C2	Re1	178.5(8)
C2	Re1	P1	95.2(3)		C8	N2	P1	121.8(6)
C3	Re1	P1	97.1(3)		N1	C4	C5	123.1(8)
C1	Re1	P1	170.9(3)		N1	C8	N2	118.4(7)
N1	Re1	P1	78.38(18)		N1	C8	C7	122.3(7)
C2	Re1	Br1	176.7(3)		N2	C8	C7	119.3(8)
C3	Re1	Br1	94.9(3)		C6	C7	C8	119.0(8)
C1	Re1	Br1	87.7(3)		C7	C6	C5	118.5(9)
N1	Re1	Br1	81.11(17)		C4	C5	C6	119.4(8)
P1	Re1	Br1	86.12(6)		C11	C9	C10	110.9(9)
N2	P1	C9	102.5(4)		C11	C9	P1	112.9(7)
N2	P1	C12	105.4(5)		C10	C9	P1	114.6(7)
C9	P1	C12	106.8(5)		C13	C12	C14	112.7(10)
N2	P1	Re1	99.6(3)		C13	C12	P1	111.4(8)
C9	P1	Re1	119.0(3)		C14	C12	P1	110.4(8)
C12	P1	Re1	120.6(4)					

Table 6 Hydrogen Bonds for κ^2-([$(CH_3)_2CH]_2$P)NH(NC_5H_4)Re$(CO)_3$Br						
D	**H**	**A**	**d(D-H) (Å)**	**d(H-A) (Å)**	**d(D-A) (Å)**	**D-H-A (°)**
C7	H7	Br1[1]	0.93	2.90	3.674(9)	141.0
C5	H5	O2[2]	0.93	2.62	3.548(11)	173.4
C9	H9	Br1	0.98	2.87	3.572(10)	129.7

Torsion Angles for κ^2-([$(CH_3)_2CH]_2$P)NH(NC_5H_4)Re$(CO)_3$Br										
A	**B**	**C**	**D**	**Angle/˚**		**A**	**B**	**C**	**D**	**Angle/˚**
C9	P1	N2	C8	137.5(8)		N1	C4	C5	C6	1.0(15)
C12	P1	N2	C8	-111.0(8)		C7	C6	C5	C4	-1.3(15)
Re1	P1	N2	C8	14.7(8)		N2	P1	C9	C11	179.6(8)
C8	N1	C4	C5	-0.9(13)		C12	P1	C9	C11	69.0(9)
Re1	N1	C4	C5	-174.2(7)		Re1	P1	C9	C11	-71.9(8)
C4	N1	C8	N2	-178.4(8)		N2	P1	C9	C10	51.3(9)
Re1	N1	C8	N2	-5.0(10)		C12	P1	C9	C10	-59.2(9)
C4	N1	C8	C7	1.1(12)		Re1	P1	C9	C10	159.9(7)
Re1	N1	C8	C7	174.6(6)		N2	P1	C12	C13	168.2(8)
P1	N2	C8	N1	-8.3(11)		C9	P1	C12	C13	-83.4(9)
P1	N2	C8	C7	172.1(7)		Re1	P1	C12	C13	56.8(10)
N1	C8	C7	C6	-1.5(13)		N2	P1	C12	C14	42.2(9)
N2	C8	C7	C6	178.1(9)		C9	P1	C12	C14	150.7(8)
C8	C7	C6	C5	1.5(14)		Re1	P1	C12	C14	-69.2(9)

Hydrogen Atom Coordinates (Å×10^4) and Isotropic Displacement Parameters (Å^2×10^3) for κ^2-([$(CH_3)_2CH]_2$P)NH(NC_5H_4)Re$(CO)_3$Br				
Atom	***x***	***y***	***z***	**U(eq)**
H4	4929.32	9026.18	4149.11	40
H7	4864.54	5398.66	6446.55	40
H6	5553.33	6490.55	6189.26	46
H5	5572.37	8366.83	5043.07	49
H9	3542.85	4734.06	3799.18	47
H10A	3123.39	3150.97	4869.42	89
H10B	3181.56	4115.69	5876.68	89
H10C	3609.57	3479.07	5318.34	89
H11A	2773.02	4497.23	3519.29	90
H11B	2916.93	5980.78	3318.4	90
H11C	2671.88	5580.78	4417.65	90
H12	3139.86	6167.62	6536.53	60
H13A	2681.22	8094.82	6502.84	99
H13B	2648.61	7281.58	5401.43	99
H13C	2943.44	8579.84	5451.55	99
H14A	3357.63	7982.98	7667.72	82
H14B	3692.12	8450.6	6739.55	82

H14C	3771.88	7087.2	7339.52	82

Appendix D: Complete Crystallographic Data Set for $[\kappa^2\text{-}[([(CH_3)_2CH]_2PO)NH(NC_5H_4)]_2MnBr]^{1+}$ Br^-

Bond Lengths for $[\kappa^2\text{-}[([(CH_3)_2CH]_2PO)NH(NC_5H_4)]_2MnBr]^{1+}$ Br^-						
Atom	**Atom**	**Length (Å)**		**Atom**	**Atom**	**Length (Å)**
Br1	Mn1	2.4378(14)		N4	C22	1.352(10)
Mn1	O1	2.062(6)		C1	C3	1.505(14)
Mn1	O2	2.081(5)		C1	C2	1.525(12)
Mn1	N2	2.316(6)		C4	C5	1.516(13)
Mn1	N4	2.321(6)		C4	C6	1.522(12)
P1	O1	1.480(6)		C7	C8	1.386(10)
P1	N1	1.662(6)		C8	C9	1.388(11)
P1	C1	1.807(8)		C9	C10	1.367(12)
P1	C4	1.810(9)		C10	C11	1.346(12)
P2	O2	1.502(5)		C12	C14	1.514(13)
P2	N3	1.664(6)		C12	C13	1.544(13)
P2	C12	1.806(9)		C15	C17	1.528(12)
P2	C15	1.810(8)		C15	C16	1.529(11)
N1	C7	1.388(9)		C18	C19	1.393(11)
N2	C7	1.339(9)		C19	C20	1.378(12)
N2	C11	1.370(10)		C20	C21	1.375(12)
N3	C18	1.392(10)		C21	C22	1.324(12)
N4	C18	1.340(10)				

Bond Angles for $[\kappa^2\text{-}[([(CH_3)_2CH]_2PO)NH(NC_5H_4)]_2MnBr]^{1+}$ Br^-								
Atom	**Atom**	**Atom**	**Angle (˚)**		**Atom**	**Atom**	**Atom**	**Angle (˚)**
O1	Mn1	O2	135.1(2)		C18	N4	C22	116.8(6)
O1	Mn1	N2	85.7(2)		C18	N4	Mn1	123.2(5)
O2	Mn1	N2	89.4(2)		C22	N4	Mn1	113.0(4)
O1	Mn1	N4	78.8(2)		C3	C1	C2	113.0(8)
O2	Mn1	N4	85.26(19)		C3	C1	P1	110.3(7)
N2	Mn1	N4	151.7(2)		C2	C1	P1	109.2(6)
O1	Mn1	Br1	112.86(18)		C5	C4	C6	113.3(8)
O2	Mn1	Br1	111.62(17)		C5	C4	P1	110.8(6)
N2	Mn1	Br1	103.97(16)		C6	C4	P1	110.0(7)
N4	Mn1	Br1	103.87(17)		N2	C7	C8	122.4(7)
O1	P1	N1	111.8(3)		N2	C7	N1	119.8(6)
O1	P1	C1	111.6(4)		C8	C7	N1	117.7(7)
N1	P1	C1	104.5(3)		C7	C8	C9	119.1(7)
O1	P1	C4	110.9(4)		C10	C9	C8	118.2(7)
N1	P1	C4	107.4(4)		C11	C10	C9	120.4(8)
C1	P1	C4	110.3(4)		C10	C11	N2	122.8(8)
O2	P2	N3	112.3(3)		C14	C12	C13	110.9(8)

O2	P2	C12	111.6(3)		C14	C12	P2	111.1(6)
N3	P2	C12	103.3(4)		C13	C12	P2	109.9(7)
O2	P2	C15	110.9(3)		C17	C15	C16	113.0(7)
N3	P2	C15	109.2(4)		C17	C15	P2	112.5(6)
C12	P2	C15	109.4(4)		C16	C15	P2	111.6(6)
P1	O1	Mn1	132.9(3)		N4	C18	N3	118.3(6)
P2	O2	Mn1	128.1(3)		N4	C18	C19	122.4(7)
C7	N1	P1	127.8(5)		N3	C18	C19	119.2(7)
C7	N2	C11	117.1(6)		C20	C19	C18	118.5(7)
C7	N2	Mn1	129.9(5)		C21	C20	C19	118.1(8)
C11	N2	Mn1	112.8(5)		C22	C21	C20	120.5(8)
C18	N3	P2	127.0(5)		C21	C22	N4	123.6(8)

Hydrogen Bonds for $[\kappa^2$-$[([(CH_3)_2CH]_2PO)NH(NC_5H_4)]_2MnBr]^{1+}$ Br^-						
D	**H**	**A**	**d(D-H) (Å)**	**d(H-A) (Å)**	**d(D-A) (Å)**	**D-H-A (°)**
C1	H1A	$Br2^1$	0.99	3.07	3.817(8)	133.0
C2	H2B	$Br1^2$	0.97	3.08	3.980(10)	155.0
C5	H5A	$Br1^3$	0.97	2.94	3.884(9)	163.2
C5	H5B	$Br2^1$	0.97	3.14	3.922(9)	139.0
C10	H10	$Br2^4$	0.94	2.96	3.784(9)	146.5
C11	H11	O2	0.94	2.53	3.099(9)	119.3
C13	H13A	$Br1^5$	0.97	3.12	4.079(11)	172.1
C21	H21	$Br2^6$	0.94	2.99	3.769(8)	140.7

Torsion Angles for $[\kappa^2$-$[([(CH_3)_2CH]_2PO)NH(NC_5H_4)]_2MnBr]^{1+}$ Br^-										
A	**B**	**C**	**D**	**Angle (˚)**		**A**	**B**	**C**	**D**	**Angle (˚)**
N1	P1	O1	Mn1	25.0(6)		N1	C7	C8	C9	-176.8(7)
C1	P1	O1	Mn1	141.6(5)		C7	C8	C9	C10	-2.4(12)
C4	P1	O1	Mn1	-94.9(5)		C8	C9	C10	C11	1.0(14)
N3	P2	O2	Mn1	-17.5(6)		C9	C10	C11	N2	0.0(14)
C12	P2	O2	Mn1	-132.9(5)		C7	N2	C11	C10	0.4(12)
C15	P2	O2	Mn1	105.0(5)		Mn1	N2	C11	C10	175.7(7)
O1	P1	N1	C7	-44.4(7)		O2	P2	C12	C14	53.3(8)
C1	P1	N1	C7	-165.3(7)		N3	P2	C12	C14	-67.6(7)
C4	P1	N1	C7	77.5(7)		C15	P2	C12	C14	176.3(6)
O2	P2	N3	C18	49.3(7)		O2	P2	C12	C13	-69.8(7)
C12	P2	N3	C18	169.6(6)		N3	P2	C12	C13	169.4(7)
C15	P2	N3	C18	-74.1(7)		C15	P2	C12	C13	53.2(7)
O1	P1	C1	C3	-62.0(7)		O2	P2	C15	C17	-52.6(7)
N1	P1	C1	C3	59.0(7)		N3	P2	C15	C17	71.6(7)
C4	P1	C1	C3	174.2(7)		C12	P2	C15	C17	-176.1(6)
O1	P1	C1	C2	62.8(8)		O2	P2	C15	C16	179.2(6)
N1	P1	C1	C2	-176.2(7)		N3	P2	C15	C16	-56.5(7)
C4	P1	C1	C2	-61.0(8)		C12	P2	C15	C16	55.8(7)
O1	P1	C4	C5	161.9(6)		C22	N4	C18	N3	179.6(7)

N1	P1	C4	C5	39.4(7)		Mn1	N4	C18	N3	-31.9(9)
C1	P1	C4	C5	-73.9(7)		C22	N4	C18	C19	-2.8(11)
O1	P1	C4	C6	35.8(7)		Mn1	N4	C18	C19	145.7(6)
N1	P1	C4	C6	-86.7(7)		P2	N3	C18	N4	-21.5(10)
C1	P1	C4	C6	160.0(6)		P2	N3	C18	C19	160.9(6)
C11	N2	C7	C8	-1.9(11)		N4	C18	C19	C20	1.6(12)
Mn1	N2	C7	C8	-176.3(5)		N3	C18	C19	C20	179.2(8)
C11	N2	C7	N1	177.8(7)		C18	C19	C20	C21	1.0(13)
Mn1	N2	C7	N1	3.4(10)		C19	C20	C21	C22	-2.3(14)
P1	N1	C7	N2	30.3(10)		C20	C21	C22	N4	1.0(14)
P1	N1	C7	C8	-150.0(6)		C18	N4	C22	C21	1.6(12)
N2	C7	C8	C9	3.0(11)		Mn1	N4	C22	C21	-150.1(7)

Hydrogen Atom Coordinates (Å×10^4) and Isotropic Displacement Parameters (Å^2×10^3) for [κ^2-[([(CH$_3$)$_2$CH]$_2$PO)NH(NC$_5$H$_4$)]$_2$MnBr]$^{1+}$ Br$^-$

Atom	*x*	*y*	*z*	U(eq)
H1	-435.78	5890.85	7480.73	36
H3	6348.21	5525.36	7683.57	37
H1A	-317.11	6732.13	9443.63	47
H2A	1610.46	5681.93	10732.22	93
H2B	472.86	6412.44	11201.7	93
H2C	1478.1	7079.65	10494.54	93
H3A	-976.7	4795.72	9008.02	91
H3B	-1055.56	4988.71	10272.62	91
H3C	55.77	4235.48	9785.17	91
H4	2361.44	7666.93	8962.83	51
H5A	1565.35	9103.2	7864.92	77
H5B	415.81	8259.25	8116.07	77
H5C	1098.29	8151.54	6995.19	77
H6A	3022.2	6824.8	6886.87	85
H6B	3813.84	6632.52	7962.96	85
H6C	3665.57	7941.25	7465.46	85
H8	-713.57	6315.76	5601.55	39
H9	-304.33	5588.75	3861.73	47
H10	1375.77	4307.33	3639.17	52
H11	2544.45	3719.15	5081.24	45
H12	7100.3	5391.68	5785.94	46
H13A	6819.76	4935.6	3973.85	100
H13B	5537.28	4278.75	4187.33	100
H13C	6802.67	3683.46	4588.56	100
H14A	5743.51	6739.84	4919.21	79
H14B	5371.88	6607.53	6146.55	79
H14C	4587.14	5934.62	5236.14	79
H15	6626.79	2390.26	5902.76	41
H16A	8561.59	2362.89	6785.65	80

H16B	8163.31	3469.88	7510.98	80
H16C	8319.83	3640.25	6250.24	80
H17A	5367.02	1612.97	7252.21	77
H17B	6282.32	2132.16	8153.22	77
H17C	6736.49	1094.98	7373.06	77
H19	6693.46	5633.66	9590.87	42
H20	5904.29	5150.31	11290.14	56
H21	4288.64	3760.13	11378.43	53
H22	3432.1	3001.42	9869.39	42